Engineering an [FeFe]-hydrogenase: do accessory clusters influence O_2 resistance and catalytic bias?

Giorgio Caserta, Cécilia Papini, Agnieszka Adamska-Venkatesh, Ludovic Pecqueur, Constanze Sommer, Edward Reijerse, Wolfgang Lubitz, Charles Gauquelin, Isabelle Meynial Salles, Debajyoti Pramanik, et al.

Engineering an [FeFe]-hydrogenase: do accessory clusters influence O_2 resistance and catalytic bias?

Giorgio Caserta,[a†‡] Cecilia Papini,[a‡] Agnieszka Adamska-Venkatesh,[b] Ludovic Pecqueur,[a] Constanze Sommer,[b] Edward Reijerse,[b] Wolfgang Lubitz,[b] Charles Gauquelin,[c] Isabelle Meynial-Salles,[c] Debajyoti Pramanik,[d] Vincent Artero,[d] Mohamed Atta,[d] Melisa del Barrio,[c] Bruno Faivre,[a] Vincent Fourmond,[e] Christophe Léger,[e] Marc Fontecave[a*]

[a] Laboratoire de Chimie des Processus Biologiques, Collège de France, Université Pierre et Marie Curie, CNRS UMR 8229, PSL Research University, 11 place Marcelin Berthelot,75005 Paris, France. [b] Max-Planck-Institut für Chemische Energiekonversion, Stiftstrasse 34-36, 45470 Mülheim an der Ruhr, Germany. [c] LISBP, Université de Toulouse, CNRS, INRA, INSA, Toulouse, France. [d] Laboratoire de Chimie et Biologie des Métaux, Université Grenoble Alpes, CEA/BIG, CNRS, 17 rue des martyrs, 38000 Grenoble, France. [e] Aix Marseille University, CNRS, BIP UMR 7281, Marseille, France

Keywords: hydrogenase, Megasphera elsdenii, H cluster, O_2 sensitivity, catalytic bias

Abstract: [FeFe]-hydrogenases, HydAs, are unique biocatalysts for proton reduction to H_2. However, they suffer from a number of drawbacks for biotechnological applications: size, number and diversity of metal cofactors, oxygen sensitivity. Here we show that HydA from *Megasphaera elsdenii* (MeHydA) displays significant resistance to O_2. Furthermore, we produced a shorter version of this enzyme (MeH-HydA), lacking the N-terminal domain harbouring the accessory FeS clusters. As shown by detailed spectroscopic and biochemical characterization, MeH-HydA displays the following interesting properties. First, a functional active site can be assembled in MeH-HydA *in* vitro, providing the enzyme with excellent hydrogenase activity. Second, the resistance of MeHydA to O_2 is conserved in MeH-HydA. Third, MeH-HydA is more biased towards proton reduction than MeHydA, as the result of the truncation changing the rate limiting steps in catalysis. This work shows that it is possible to engineer HydA to generate an active hydrogenase that combines the resistance of the most resistant HydAs and the simplicity of algal HydAs, containing only the H-cluster.

Introduction

Water splitting to hydrogen and oxygen is one of the few promising strategies for storing renewable, intermittent and diluted energies at large scale. In particular, the development of industrially relevant energy conversion (photo)-electrochemical systems, such as electrolyzers, photoelectrochemical cells and fuel cells, will depend on our ability to use earth-abundant elements exclusively and to optimize cheap, stable and efficient catalysts for the redox reactions at the electrodes. Current research in this direction targets both synthetic solid and molecular catalysts. However, enzymes are also extensively studied (e.g. for use in bioelectrodes) since they display remarkable performances in particular with respect to turnover frequencies (TOFs), far exceeding those displayed by synthetic catalysts. This is especially true for hydrogenases which catalyze the interconversion of molecular hydrogen into protons and electrons with TOF values up to 10^4 s^{-1}.[1] These enzymes operate under mild conditions and close to the thermodynamic reaction equilibrium, i.e. with very little overpotential. There

are two classes of hydrogenases, the [NiFe]-hydrogenases and the [FeFe]-hydrogenases, based on the metal content of their respective active site.[1,2] The work presented here deals exclusively with the second class.

Only two fully active forms of [FeFe]-hydrogenases, named HydAs in the following, have been structurally characterized so far: HydA from *Clostridium pasteurianum* (CpHydA)[3] and HydAB from *Desulfovibrio desulfuricans* (DdHydAB).[4] These studies have established that the enzyme active site (referred to as the H-cluster) consists of a diiron center (referred to as the 2Fe-subcluster) sharing a cysteine ligand with a [4Fe-4S] cluster (Scheme 1). Each Fe atom of the 2Fe-subcluster has one CO and one CN^- ligand and is connected to the other through a bridging CO ligand. The coordination sphere is completed by a unique azapropanedithiolate (adt^{2-}) ligand bridging the two Fe atoms.[5–8] Most HydAs contain accessory [4Fe-4S] and [2Fe-2S] ferredoxin-like clusters that electronically connect the active site to the protein surface. For example, clostridial HydAs contain four accessory [Fe-S] centers while DdHydAB and *Megasphaera elsdenii* HydA (MeHydA) contain two ferredoxin-like [4Fe-4S] clusters.[3,4,9] In contrast, [FeFe]-hydrogenases from green algae, such as *Chlamydomonas reinhardtii* (CrHydA), only contain the catalytic H-cluster and no accessory clusters[10], thus representing the simplest form of [FeFe]-hydrogenases yet identified. So far no three-dimensional structures of fully mature members of that specific class have been obtained.

Scheme 1: Schematic representation of the active site of [FeFe]-hydrogenases. The dashed circle indicates the vacant coordination position on the distal iron of the 2Fe-subcluster.

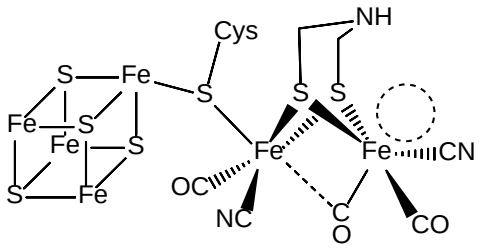

Despite their high catalytic efficiency, [FeFe]-hydrogenases are nevertheless fraught with a number of drawbacks which still need to be addressed before they can be implemented into biotechnological devices. The first one resides in the complexity of their metal centers and the need for complex protein machineries for their expression and maturation.[11] Recently, we have discovered an efficient chemical maturation technology which provides an exquisite solution to this issue.[6,12] The second one resides in the limited tolerance of HydAs to molecular oxygen, which varies significantly from one enzyme to another.[13] Current research aims at understanding the molecular basis of the reaction of HydA with O_2[14–16] and at finding strategies for improving stability.[17] The third one concerns the size of HydA proteins, which severely limits enzyme density at the surface of the electrodes. In this context, CrHydA, the smallest enzyme, is an interesting hydrogenase. Unfortunately, it belongs to the most O_2-sensitive ones.[13]

So far, all these issues have been addressed using a very limited set of HydAs, almost exclusively CrHydA, CpHydA and, to a lesser extent, DdHydAB. Having recently invested significant efforts in the heterologous expression and characterization of MeHydA[9], we have studied its reactivity towards O_2 using a previously developed electrochemical method and found it to be, when adsorbed to an electrode, the most O2-resistant HydA reported so far, through direct experimental comparison with CrHydA and the enzyme from *Clostridium acetobutylicum* CaHydA. Furthermore, considering the great O_2-sensitivity of CrHydA, it has been sometimes suggested that the accessory clusters might contribute to protect the active site from O_2 attack via delivering electrons to the active site.[13,17] Thus, we also report the results obtained with the first fully characterized and active truncated form of HydA from *Megasphaera elsdenii* (named MeH-HydA), in which the ferredoxin domain has been deleted and thus containing the H-cluster exclusively. While retaining a well-assembled and active H-cluster, MeH-HydA displays specific electrochemical properties. Interestingly, the O_2-resistance of MeHydA is retained in MeH-HydA, so that MeH-HydA displays greatly reduced reactivity with respect to O_2 as compared to CrHydA. Furthermore, the truncation results in an enzyme much more biased towards H2 production, raising new hypothesis regarding the role of the accessory clusters in tuning the bias of HydAs.

Methods

MeHydA was purified, reconstituted and activated as previously described.[9] $[Fe_2(adt)(CO)_6]$ (adt^{2-} = 2-aza-propane-1,3-dithiolate) and $[Fe_2(pdt)(CO)_6]$ (pdt^{2-} = propane-1,3-dithiolate) were synthesized according to literature procedures.[18] Preparation of CrHydA was performed as previously described.[6,19] Protein concentrations were determined with the Bradford assay (Bio-Rad), using bovine serum albumin as a standard.

Preparation of CaHydA

E. coli MG1655ΔiscR::kan strain was obtained by generalized P1 phage- transduction from the JW2515-3 strain from Keio Collection (ECK2528).[20] Removal of kanamycin resistance cassette was by Flp recombinase expressed from pCP20 plasmid[21] leaving an FRT scar and yielding the *E. coli MG1655ΔiscR::FRT* strain.

p*thlA*-CaHydA-LL-C-Tag plasmid was constructed by replacing the PH (*C. acetobutylicum* hydrogenase) promoter by the *thlA* (*C. acetobutylicum* thiolase) promoter from $pThydA_{Ca}$-C-tag[22] in the pPH_CaHydA-LL-C-Tag plasmid.[23]

C. acetobutylicum maturation proteins genes (*hydE*, *hydF* and *hydG* genes) were PCR amplified from *C. acetobutylicum* ATCC 824 genomic DNA and further cloned as a single operon in the pACYC184 plasmid (Gene bank accession X06403) under the P_R [24] promoter dependence, yielding to the custom pACYC_Mat plasmid.

Constructed plasmids and newly generated operons were validated by restriction profile and sequencing, respectively, before to be introduced in the *E. coli MG1655ΔiscR::FRT* strain.

CaHydA expression was performed with *E. coli MG1655ΔiscR::FRT* strain containing both p*thlA*-CaHydA-LL-C-Tag and pACYC_Mat plasmids. This strain was used since overexpression of the *isc* operon (by deleting the *iscR* negative regulator) stimulated the Fe-S cluster assembly process leading to higher specific and total recombinant hydrogenase activity.[25] The recombinant strain was grown in custom "MAC" medium (Tryptone 10g/L, Yeast extract 5g/L, HEPES 23 g/L, nitrilotriacetic acid 0.2 g/L, NaCl 2 g/L, K_2HPO_4 0.5 g/L, $FeSO_4$ 0.05 g/L, pH 7.3), packed in 500 mL bottles and sparged with pure nitrogen for 40 minutes before sterilization. Medium was supplemented with glucose (20 g/L final), ammonium ferric citrate (2 mM final), sodium fumarate (25 mM final), sodium nitrate (10 mM final), cysteine (0.32 g/L final) and carbenicillin (100 µg/mL final) and chloramphenicol (30 µg/mL final) prior to inoculation. Cultures were inoculated at 0.05 OD_{600nm} and incubated at 30°C. Cultures reaching OD_{600nm} > 3 (after around 16 hours) were transferred to an anaerobic Jacomex glove box filled with 100% N_2 atmosphere. Cells were collected by centrifugation at 8000 g for 10 min at 4°C, resuspended in buffer (Tris HCl 100 mM, NaCl 150 mM, Glycerol 10%, pH 7.6, DTT 2 mM) and concentrated 30 times. Cells were either stored at -20°C or directly used for enzyme purification.

Protein extraction, hydrogenase purification and purified enzyme purity control were finally performed as previously described.[23]

Preparation of MeH-HydA

Molecular biology. The pT7-7-derived plasmid containing the whole hydrogenase gene (pT7-7-Me-HydA)[26] was used to amplify by PCR and clone into pT7-7 the gene fragment encoding the 405 amino acid residues. This gene fragment lacks the N-terminal part which harbors the ferredoxin domain (methionine 1 to valine 80). The PCR fragment was purified with the High Pure PCR kit (Roche Applied Science), double-digested with NdeI and PstI (Thermo Fisher Scientific) and gel-purified before direct cloning into the pT7-7 expression vector, leading to the pT7-7-MeH-HydA plasmid. Chemically competent DH5α cells were transformed with the plasmid and gene integrity was verified by DNA sequencing.

Expression and purification of MeH-HydA. TunerDE3 cells transformed with the pT7-7-MeH-HydA plasmid were grown in Terrific Broth medium supplemented with ampicillin at 37 °C, until the optical density at 600 nm reached 0.5. Protein synthesis was induced by the addition of isopropyl β-D-thiogalactopyranoside to a final concentration of 0.5 mM. Cells were grown for an additional 5-6 h at 20 °C to avoid the formation of inclusion bodies. Cells were harvested by centrifugation and stored at -80°C until use. Cells were re-suspended in Tris–HCl Buffer 50 mM pH 8.0 containing 300 mM NaCl, 0.5 % v/v Triton and discontinuously sonicated for 10-12 min in a water/ice bath. Cellular extracts were centrifuged for 1h at 193000 g and the soluble fraction was loaded on a HisTrap crude FF column (GE-healthcare) equilibrated with 50 mM Tris–HCl pH 8.0, 300 mM NaCl (Buffer A). After extensive wash with 50 mM Tris–HCl pH 8.0, 300 mM NaCl, 10 mM imidazole, the protein was eluted with a linear gradient of Buffer A supplemented with 500 mM imidazole. Fractions containing apo-MeH-HydA were pooled after the addition of 5 mM DTT, concentrated by ultrafiltration and loaded on a Superdex S200 16-600 equilibrated in 50 mM Tris–HCl pH 8.0, 300 mM NaCl, 10 % w/v glycerol, 5 mM DTT. Only fractions corresponding to the monomer were combined and concentrated giving a pure and homogeneous protein. Finally, the apo-protein was concentrated to 5-10 mg/ml, flash-frozen in liquid nitrogen and stored at -80 °C until use.

Reconstitution of the [4Fe-4S] cluster. The iron-sulfur cluster reconstitution was conducted under strictly anaerobic conditions in a glove box (M Braun) with less than 0.5 ppm O_2. After incubation of apo-protein (100 µM) with 10 mM DTT for 15-20 min at 20°C, a 5-5.5 molar excess of $[(NH_4)_2Fe(SO_4)_2,6H_2O]$ and L-cysteine was added, followed by the addition of a catalytic amount of the *E. coli* cysteine desulfurase CsdA (1–2 % molar equivalent). Cysteine desulfurase was prepared as reported.[27] The reaction was performed overnight and the cluster assembly reaction was monitored by recording UV–visible absorption spectra every 20 min. The reconstituted protein, called FeS-MeH-HydA, was then centrifuged 20 min at 12000 rpm and purified on Superdex S200 10/300 GL equilibrated with the reconstitution buffer (50 mM Tris-HCl pH 8.0, 300 mM NaCl, 10 % w/v glycerol) supplemented with 5 mM DTT. A pure and homogeneous fraction was collected, concentrated with Amicon Ultra 30-kDa centrifugation filters (Millipore) and stored at -80 °C in sealed vials under nitrogen atmosphere until use. For Mössbauer characterization the same procedure was followed but using $^{57}Fe(SO_4)$ as a source of Fe, a 0.62 M solution of $^{57}Fe(SO_4)$ in sulfuric acid diluted to 0.023 M in 1.0 M Tris-HCl buffer pH 8.0. For each sample, the Fe and S content was determined 3 times for 2 different protein concentrations according to the methods of Fish[28] and Beinert[29] respectively.

Activation of MeH-HydA. In a standard experiment, protein solutions were extensively washed with 100 mM potassium phosphate pH 6.8 to remove DTT traces and avoid DTT-dependent decomposition of the organometallic chemicals. Initially, maturation of FeS-MeH-HydA was conducted as reported for the full length protein[9] : 50 µM protein solution in 100 mM potassium phosphate

pH 6.8 was incubated for 1h with 3-10 equivalents of $[Fe_2(adt)(CO)_4(CN)_2]^{2-}$. Excess of the chemical was removed using a desalting column (NAP-10, GE healthcare). Maturation was verified by assaying the hydrogenase activity of the protein. A specific activity of 23 ± 3.5 µmol H_2.mg^{-1}.min^{-1} was obtained, a value 30-fold lower than that of active MeHydA. Fe and S assays proved that only very little complex was incorporated into the protein, as confirmed by FTIR spectroscopy. Optimization of the procedure was achieved by varying the temperature, the incubation time, the excess of the synthetic complex $[Fe_2(adt)(CO)_4(CN)_2]^{2-}$ and the pH of both the maturation mix, from 8 to 5, and the activity assay (Table S1). A shift of the pH to 6.0 produced a strong enhancement of the hydrogenase activity with a specific activity of 125 ± 15 µmol H_2.mg^{-1}.min^{-1}. The specific activity was slightly improved to 135 ± 10 µmol H_2.mg^{-1}.min^{-1} when the excess of the chemical was removed. These new maturation conditions were used to prepare active MeH-HydA for spectroscopic studies. The same protocol was used for reconstituting MeH-HydA with $[Fe_2(pdt)(CO)_4(CN)_2]^{2-}$.

Hydrogenase activity assay. H_2 production was determined according to a published procedure[6] by using methyl viologen as an electron mediator and sodium dithionite as the reducing agent. Briefly, in all enzymatic assays as reported in Table S1 MeH-HydA (5−10 µL) corresponding to 0.2 nmol of hydrogenase was added to a total amount of 1.11 mL of 100 mM potassium phosphate, pH 6.8, 100 mM sodium dithionite, and 10 mM methyl viologen in a 10 mL vial sealed under anaerobic conditions (rubber stoppers, Carl Roth). Gas chromatograms were recorded on a GC System (Shimadzu GC-2014 with a thermal conductivity detector and a Quadrex column) and the amount of H_2 was quantified using a calibration curve. $[Fe_2(adt)(CO)_4(CN)_2]^{2-}$ and FeS-MeHydA were assayed as controls and did not show any detectable activity. All activities in this study were measured at least twice on 3 different protein preparations.

Spectroscopic methods. Pulse EPR spectra were recorded at Q-band (34 GHz) on a Bruker Elexsys E580 spectrometer equipped with a dedicated Q-band super-QFT bridge. The 30 µl samples were accommodated in a homebuilt TE011 resonator.[30] Cryogenic temperatures (10-20K) were reached using a custom made Helium closed cycle cryostat from Cryogenic Ltd. EPR signals were measured using FID detection following a 1µs excitation pulse.[31] For the interpretation of all EPR experimental data, a home written simulation program (based on the EasySpin package[31]) in MATLAB™ was used.

FTIR measurements were performed on a BRUKER IFS 66 v/s FTIR spectrometer equipped with a Bruker MCT (mercury cadmium telluride) detector. The spectra were accumulated in the double-sided, forward-backward mode with 1000 scans (14 minutes) and a resolution of 2 cm-1 at 15 C. Data processing was facilitated by home written routines in the MATLAB™ programming environment. To obtain Hox-CO state sample was flushed with carbon monoxide for 20 minutes. Similarly, to isolate the Hox state the sample was flushed for 30 hours with argon gas. To access the reduced states the sample was flushed with hydrogen for few hours and treated with 10mM sodium dithionite buffer.

Mössbauer spectra were recorded on a conventional spectrometer with alternating constant acceleration of the γ-source. The sample temperature was maintained constant in an Oxford Instruments Variox cryostat. Isomer shifts are quoted relative to iron metal at 300 K. Mössbauer spectra were collected for frozen aqueous solution sample (2 mM, 650 µL) at 160 K and fitted using the program MFIT (written by Eckhard Bill, Max Planck Institute for Chemical Energy Conversion) with Lorentzian doublets.

Electrochemistry. All electrochemical experiments were carried out in a glove box (JACOMEX) filled with N_2. The homemade pyrolytic graphite edge electrode was mounted onto a PINE MSR rotator. The potentiostat was model PGSTAT128N from METROHM. The buffer used in the electrochemistry experiments was a mixture of MES, CHES, HEPES, TAPS and Na-acetate, 5 mM each, plus NaCl 0.1M, titrated to pH 5, 7 or 9. In voltammetric experiments where the pH and H_2 concentration were varied, intermediate pH values were obtained by mixing various amounts of these stock solutions, and partial pressures of H_2 in the range 0.18-1 bar were obtained by bubbling in the electrochemical cell a mixture of H_2 and Ar, the composition of which was adjusted using mass flow controllers (model SLA5800 from BROOKS Instruments). Circulating water in the double jacket of the electrochemical cell regulated the temperature. The open circuit potential (OCP) was measured before each experiment to make sure that the desired pH and partial pressure of H_2 had been obtained; the reproducibility of the OCP between independent experiments was better than 4 mV. The contribution of the capacitive current was removed by averaging the forward and backward scans and offsetting the resulting signal so that the OCP was the same as that measured before recording the voltammogram.

The CO-inhibition electrochemical data were corrected for film loss[32] and fitted with the program QSoas[33] (www.qsoas.org), using the text file model "A<=>I [ki*co][ka]" and the command "QSoas> fit-kinetic-system model.txt /with=co:2,exp,common" where A and I stand for "active" (CO-free) and "inactive" (CO-bound), "2" is the number of successive injections of CO in the experiment, "common" means that the time constants for the exponential decay of [CO] after each injection are the same. "model.txt" is the text file that contains the kinetic model. Aerobic inactivation is studied in direct electrochemistry as for CO inhibition, although the time-dependent concentration of O_2 is easily measured using a 2nd rotating electrode poised at low potential.[13] This makes it easy to measure the time constant for the decay of the concentration of O_2, which is used to constrain the fitting procedure.

Results

Preparation of MeH-HydA, the truncated form of HydA from *M. elsdenii*.

Figure S1 shows an alignment of the amino acid sequences of MeHydA and CpHydA. Both contain two ferredoxin-like clusters, each within a cysteine-rich CxxCxxCxxxC motif, in the N-terminal domain. The significant degree of identity (40%) between the two proteins and the fact that CpHydA has been characterized by X-ray crystallography allowed the identification of potential sites for protein truncation, in order to remove the accessory clusters. The chosen truncated protein, named MeH-HydA, thus starts at residue V80 of MeHydA, corresponding to residue 208 in CpHydA between the β-strand 10 and α-helix 6.[3] MeH-HydA has a theoretical molecular weight of 45.8 kDa and is designed to harbor the H-cluster exclusively. To facilitate purification a hexahistidine tag was added at the N-terminus. Plasmid preparation, expression and aerobic purification of apo-MeH-HydA are described in the supplementary information section (see Figure S2). Approximately 15 mg protein could be obtained from 1 L of culture. Gel filtration experiments showed that apo-MeH-HydA is a monomer in solution (Figure S2).

The purified protein contained negligible amounts of Fe (<0.2 ± 0.1 Fe per polypeptide chain) and thus was mainly in the apo-protein form. Its UV-visible light absorption spectrum displayed indeed only a very weak signal at 400 nm (Supplementary information, Figure S3a). One [4Fe-4S] cluster could be assembled upon incubation of the protein with an excess of iron ammonium sulfate and L-cysteine in the presence of dithiothreitol (DTT) and cysteine desulfurase (Supplementary information, Figure S3b and Figure S4a). The presence of a band at 400 nm (A400/A280 = 0.24) in the light absorption spectrum of the reconstituted protein (Supplementary information, Figure S4a) as well as iron and sulfur quantitation (Fe: 4.1 ± 0.2; S: 4.3 ± 0.2 per polypeptide) were consistent with the protein containing a single [4Fe-4S] cubane cluster. The cluster is EPR silent consistent with a S=0 $[4Fe\text{-}4S]^{2+}$ state and excluding the presence of paramagnetic forms of the cluster. Upon anaerobic reduction with dithionite, it could be converted into an EPR active state. The rhombic signal (g = 2.043, 1.924, 1.892) is characteristic of a single S=1/2 $[4Fe\text{-}4S]^{+}$ cluster (Supplementary information Figure S4b). Spin quantitation, using Cu-EDTA as a standard, showed that about 40 % of the clusters were reduced. Finally, the protein was characterized by Mössbauer spectroscopy after reconstitution of the cluster with ^{57}Fe. The Mössbauer spectrum is shown in Figure S4c, Supplementary information. It can be simulated with a single pure $[4Fe\text{-}4S]^{2+}$ cluster, containing two species (1:1) with parameters δ=0.31 mm/s ΔQ=0.97 mm/s and δ=0.50 mm/s ΔQ=0.98 mm/s.

These data clearly establish that, while lacking the whole N-terminal domain, MeH-HydA can properly assemble a redox-active [4Fe-4S] cluster.

Synthetic maturation of MeH-HydA: towards an active enzyme

To achieve full maturation of the protein we used the efficient chemical maturation protocol previously reported[5], which consists in the anaerobic treatment of the hydrogenase containing only the [4Fe-4S] cluster with an excess of a dinuclear iron complex, $(Et_4N)_2[Fe_2(adt)(CO)_4(CN)_2]$ (adt^{2-} = azapropanedithiolate), mimicking the 2Fe-subcluster of HydA. In the supplementary information section we describe the exact MeH-HydA maturation protocol as it slightly differs from that previously used for MeHydA, in particular because lower pH values were required for optimized enzyme activation (Table S1). Maturation was monitored by assaying the protein for its Fe content and for hydrogenase activity using the standard methyl viologen/dithionite assay in phosphate buffer pH 6.8 as well as by FTIR spectroscopy.

Thus, when the reaction was carried out over 2 hours, in 0.1 M potassium phosphate buffer, pH 6, followed by desalting to remove the excess of complex, the resulting MeH-HydA enzyme displayed a large hydrogen evolution activity, 135 ± 15 μmol H_2 mg^{-1} min^{-1} (Table S1), however lower than that of MeHydA (500 μmol H_2 mg^{-1} min^{-1}). Fe and sulfur quantitation showed that almost 50-60% of the H-cluster could be reconstituted under the best conditions. Once maturated, the protein is stable in anaerobic neutral aqueous solutions: no precipitation and no change in its light absorption spectrum could be observed after several hours at room temperature.

That the H-cluster was correctly assembled was further substantiated by spectroscopic characterization (Figure 1).

First, MeH-HydA was characterized by FTIR spectroscopy. The latter is indeed appropriate for identifying the CO (1800-2020 cm^{-1}) and CN^- (2040-2100 cm^{-1}) vibrations associated with the CO and CN^- ligands present in the 2Fe-subcluster. These signals can be clearly distinguished from those of the $[Fe_2(adt)(CO)_4(CN)_2]^{2-}$ complex free in solution which are much broader. Moreover, it allows distinguishing between different H-cluster states usually coexisting in hydrogenase preparations. The FTIR spectrum of the protein after maturation (Figure 1A, MeH-HydA and Table S2) displayed sharp peaks corresponding to CN^- and CO vibrations typical of those previously observed for MeHydA H-cluster in the Hox and Hox-CO state, in which an extra CO molecule binds the free coordination site on the 2Fe-subcluster.[9] The excess of the synthetic complex used during maturation can be indeed a source of CO, which then reversibly binds to the 2Fe-subcluster, explaining why synthetic maturation usually results in a mixture of Hox and Hox-CO states. For unambiguous assignment of the FTIR peaks we treated the protein with an excess of CO to

generate a pure Hox-CO form (Figure 1, MeH-HydA CO). For reference, we also maturated MeH-HydA with the $[Fe_2$(pdt=propanedithiolate)$(CO)4(CN)2]^{2-}$ complex since, as previously reported for CrHydA[34], only Hox can be obtained in that case (Figure 1, MeH-HydA(pdt)). Extensive exposure to Ar gas converted active MeH-HydA into (mainly) Hox (Figure 1, MeH-HydA Ar). Specifically Hox-CO and Hox are well characterized by a peak at 2012 and 1945 cm^{-1} respectively (to be compared to 2013 and 1938 cm^{-1} for MeHydA (Figure S5). Finally, treatment of active MeH-HydA with hydrogen and dithionite (DT) resulted in a complex spectrum reflecting a decoordination of CO (decrease of Hox-CO proportion) and the formation of the reduced Hred state characterized by a peaks at 1896 cm^{-1} (Figure 1, MeH-HydA H_2/DT). The presence of a peak at 1944 cm^{-1} indicates incomplete reduction. Table S2 compares the parameters obtained for MeH-HydA, MeHydA and CrHydA. Also the spectrum of as-maturated MeHydA is displayed in Figure S5 for comparison. It clearly shows that the active sites of MeHydA and CrHydA have very similar vibrational properties and furthermore that the truncation of the ferredoxin domain in MeHydA has almost no effect on these properties, demonstrating that the active site has remained intact.

Both Hox and Hox-CO states are paramagnetic and can be observed by EPR spectroscopy. In Hox, the 2Fe-subcluster is in the Fe(I)Fe(II) (S=1/2) configuration while the [4Fe–4S] is oxidized (2+ state) and thus EPR silent. While its EPR signal is rhombic, that of Hox-CO is axial. The EPR spectrum of MeH-HydA (Figure 1B) clearly shows the presence of the two species, with Hox contribution decreasing upon addition of CO. The spectra have been simulated using parameters Hox: g=(2.095, 2.039, 1.996); Hox-CO: g= (2.0196, 2.009, 2.0079) (Figures 1B and S6). Figure S6 shows that the Hox spectrum of MeH-HydA is only very slightly shifted with respect to MeHydA. In contrast, the spectrum of Hox-CO in MeH-HydA is much less anisotropic than in MeHydA.

Electrochemical characterization.

In Protein Film Voltammetry (PFV) experiments, the magnitude of the current cannot be interpreted. The current is proportional to both the turnover rate and the electroactive coverage, but the latter is most often unknown and varies from one experiment to another. Furthermore, the truncated fragment is actually the site of interaction between the WT enzyme and the electrode. We therefore expect that the electroactive coverage of the WT and truncated enzymes should be different. Irrespective of the coverage, the turnover rate of the enzyme at a certain potential also depends on the rate of interfacial electron transfer, which is affected by the truncation. The difference in the value of the current obtained with MeHydA and MeH-HydA is therefore meaningless. In PFV, the information always comes from the analysis of relative changes in current, in response to a change in e.g. substrate/inhibitor concentration or electrode potential, as illustrated below.

Reaction with carbon monoxide

We used a previously described electrochemical protocol to characterize the kinetics of the inhibition of MeHydA and MeH-HydA by the gaseous enzyme inhibitor CO. The enzymes are adsorbed on a rotating graphite disk electrode, the solution is purged with H_2 and the electrode poised at -0.16V vs SHE. Thus, the activity of the enzyme is monitored by the H_2 oxidation current, the change of which reports on the rate of inhibition. Upon injection of CO in the electrochemical cell the CO concentration suddenly increases and then is forced to return to zero as the cell solution re-equilibrates with the constant flux of H_2.[35,36] The results are shown in Figure S7: the current initially decreases, showing that indeed CO is an inhibitor of both MeHydA and MeH-HydA, and then returns to its initial value, clearly demonstrating that the inhibition by CO is reversible. In contrast, and as observed with most HydAs (but not the enzyme from *A. woodii*) [37], the inhibition by CO is partly irreversible at lower potentials (e.g. -360mV or -400 mV vs SHE, pH 7, Figure S7C); it has been argued that this is caused by the disruption of the bond between the [4Fe-4S] and 2Fe-subcluster.[36,38]

The rate constant of CO binding and release were determined by fitting a model that assumes (pseudo)first order kinetics in both directions.

$$\mathrm{A} \underset{k_{\mathrm{out}}^{\mathrm{CO}}}{\overset{k_{\mathrm{in}}^{\mathrm{CO}} \times [\mathrm{CO}]}{\rightleftharpoons}} \mathrm{I} \qquad (1)$$

The obtained rate constant values for both forms of the enzyme are shown in Table S3, together with previously published values obtained for CaHydA, CrHydA, DdHydAB and *Acetobacterium woodii* HydA. Analysis of the k_{in}^{CO} values clearly shows that inhibition by CO is slower in the case of MeHydA and MeH-HydA than with any previously investigated HydA.

Reaction with dioxygen

The same approach was used for characterizing the inhibition by O_2 quantitatively, using the 4 enzymes MeHydA, MeH-HydA, CaHydA and CrHydA. Figure 2A shows the current against time trace (in black) obtained upon exposure of MeHydA to O_2, and that (in blue) obtained with CaHydA. In both cases, like for other HydAs studied before, the reaction can only be described by a two-step mechanism[13,17,39], which assumes that the active form of the enzyme (A) reacts with O_2 during a bimolecular step to form an O_2 adduct (I), which can either be repaired or be irreversibly transformed into a dead-end species (D):

$$\mathrm{A} \underset{k_a}{\overset{k_{\mathrm{in}}^{\mathrm{O_2}} \times [\mathrm{O_2}]}{\rightleftharpoons}} \mathrm{I} \overset{k_3}{\rightarrow} \mathrm{D} \qquad (2)$$

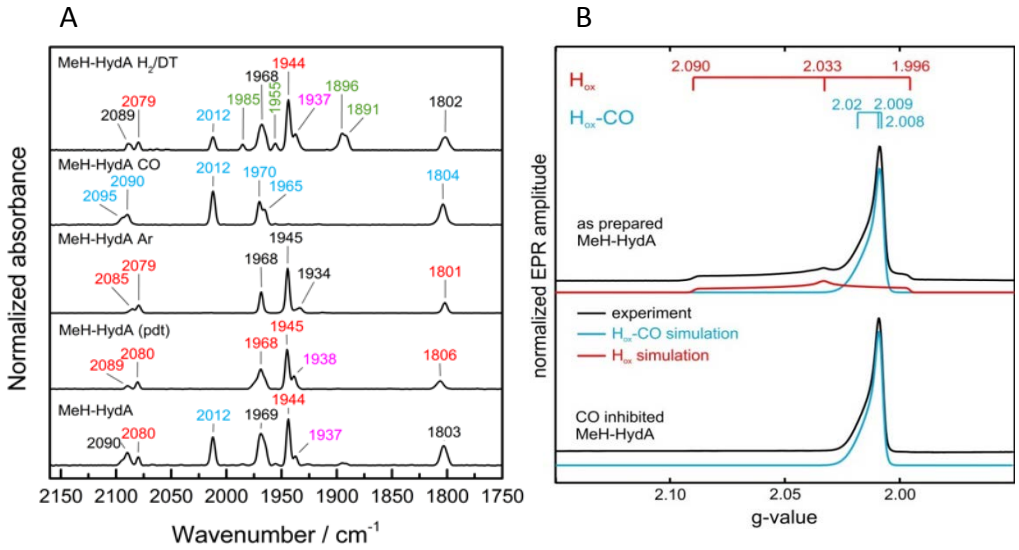

Figure 1: FTIR and EPR spectra of MeH-HydA. A) From bottom to top: FTIR spectrum of MeH-HydA maturated with $[Fe_2(adt)(CO)_4(CN)_2]^{2-}$ (H_{ox}+H_{ox}-CO); maturated with $[Fe_2(pdt)(CO)_4(CN)_2]^{2-}$ (H_{ox}); maturated with $[Fe_2(adt)(CO)_4(CN)_2]^{2-}$ and flushed with Ar (mainly H_{ox}); maturated with $[Fe_2(adt)(CO)_4(CN)_2]^{2-}$ and treated with CO (H_{ox}-CO); maturated with $[Fe_2(adt)(CO)_4(CN)_2]^{2-}$ and treated with H_2 100% and 10 mM Na-dithionite (DT) (H_{red}, $H_{red}H^+$, H_{ox}). B) Q-band FID-detected EPR spectra measured at 20K for active MeH-HydA before and after treatment with CO and their simulations. Information about signal positions is indicated and assigned to different redox states by colorcode: red indicates H_{ox}, light blue $H_{ox}CO$, green, pink and blue reduced states; and black overlaping signals.

With MeHydA we obtained the following values: k_{in}^{O2}=0.25±0.1 $mM^{-1}s^{-1}$, k_a=0.05±0.02 s^{-1}, k_3=0.015±0.007 s^{-1} and thus $k_{eff}=k_{in}^{O2}\cdot k_3/(k_a+k_3)$=0.075 $mM^{-1}s^{-1}$, k_{eff} being the "global" second-order rate of irreversible formation of the inactive forms, defining the "overall" sensitivity to O_2. The rate constants collected in Table 1 clearly show that MeHydA reacts with O_2 in the first step (k_{in}^{O2} values) much more slowly than any other HydA studied so far; the inset of Fig 2A clearly shows a difference in initial rates of reaction with O_2 of MeHydA and CaHydA. This nicely parallels the observed slow reaction of MeHydA with CO. A typical experiment showing the inhibition by O_2 of MeH-HydA is shown as a black trace in Fig 2B.

Table 1. Kinetic parameters for the reaction of HydA enzymes with O_2

	k_{in}^{O2}	k_a	k_3	$k_{eff}=k_{in}^{O2}\cdot k_3/(k_a+k_3)$	T	E	References
	$mM^{-1}s^{-1}$	s^{-1}	s^{-1}	$mM^{-1}s^{-1}$	°C	mV vs SHE	
MeHydA	0.25±0.1	0.05±0.02	0.015±0.007	0.075	20	+40	This work
MeH-HydA	n/a			0.08	20	+40	This work
CaHydA	0.9±0.2	0.07±0.02	0.004±0.00	0.05	20	+40	This work
CrHydA	2.5	0.035	0.024	1.02	12	+40	[13]
A. woodii HydA	6.5	0.005	0.0032	2.5	30	+40	[37]
DdHydAB	40	0.15	n/d	n/d	30	+200	[40]

n/a: not applicable ; n/d: not determined

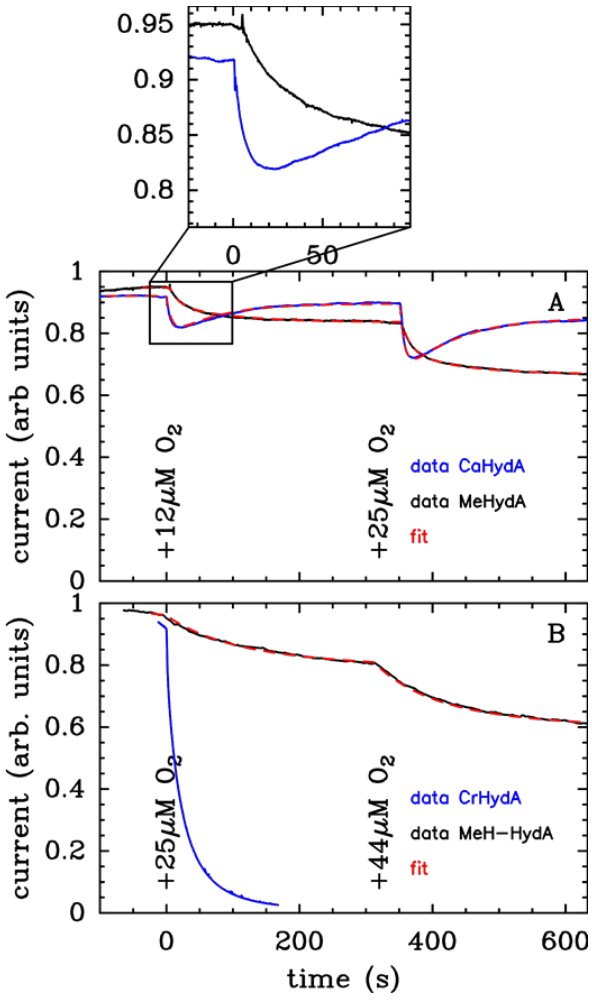

Figure 2: Aerobic inactivation of MeHydA and MeH-HydA, and comparison with CaHydA and CrHydA. The enzymes were adsorbed onto a rotating graphite electrode poised at 0.2 V, and the hydrogen oxidation current under 1 atm of H_2 was monitored following the injection of small amounts of O_2 in the electrochemical cell, as indicated. Panel A compares MeHydA (black line, corrected for film loss[32]), and CaHydA (blue). The red lines are fits of the two-step model. The inset shows that the initial rate of reaction with O_2 is much faster in the case of CaHydA than in the case of MeHydA. Panel B compares MeH-HydA and CrHydA. The red line is a fit of a simple model that assumes irreversible bimolecular reaction with O_2. T=20°C, pH=7, electrode rotation rate = 3krpm.

In contrast with all other HydAs studied so far, we obtained a good fit to the data by using a much simpler model where the enzyme merely reacts with O_2 with 2nd order kinetics to irreversibly form an inactive state, with $k_{in}^{O2} = k_{eff} = 0.08\ s^{-1}\ mM^{-1}$. This is the model used for standard [NiFe]-hydrogenases.[41] Figure 2B also shows the experimental trace in the case of CrHydA, which illustrates the great sensitivity of this enzyme with respect to O_2. These data demonstrate that MeHydA and MeH-HydA display similar limited sensitivity with regard to O_2 (from comparison of k_{eff} values), even though the kinetics of the reaction are not the same.

Catalysis

The catalytic responses (steady-state voltammograms) of MeHydA and MeH-HydA are shown in panels A and B of Figure 3. At the slow scan rates used here, the response is in a steady-state regime (it is independent of scan rate).[42]

The shapes of the signals are significantly different; in particular MeH-HydA appears to be more biased in the direction of H^+ reduction (the current is larger in the reductive direction). (Note that the bias relates to the magnitude of the current in each direction; the direction of the reaction and thus the sign of the current are defined by the sign of the difference between the electrode potential and the open circuit potential).[43] Preliminary study of a truncated form of CaHydA also showed a comparable change of the voltammograms.[23] Here we apply previous models to make sense of this change in electrochemical signature. We previously described the kinetic models that can be fitted to these data.[42,44] The simplest model, called EEC, reduces the enzyme to a two-electron active site that can directly exchange electrons with an electrode. A more complex model, EEC(R), explicitly considers a one-electron relay that mediates electron transfer between the electrode and the active site (see Figure S8 for details). Regarding MeHydA, Figures 3A and C show that the EEC(R) model fits the data much better than the EEC model (the derivatives of the data are shown in panels C and D, because simultaneously fitting a model to the data and to the derivative of the data greatly increases the reliability of the fit).[44] In contrast, for MeH-HydA both models are equivalent. This is as expected considering the cofactor content in these two enzymes, meaning that the fitting procedure can tell which of the two enzymes has accessory clusters. We have already reached this conclusion in a previous comparison of CaHydA and CrHydA.[44] The examination of the best parameters of the fits in Table S4 tells us why MeHydA is better (relatively) at oxidizing H_2 than MeH-HydA. First, for both enzymes, the fits (of the two distinct models) converge on the same values of the two one-electron potentials of the active site ($E^0_1 \simeq$ -410 mV vs SHE and $E^0_2 \simeq$ -475 mV vs SHE) and the "intrinsic" value of the bias ($k_2/k_{-2} \simeq$ 15 in the reductive direction). This is consistent with the conclusion from spectroscopy that the truncation does not affect the active site. Second, for MeHydA, the fit identifies a very slow electron transfer step in both directions (k_1 and k_{-1}), between the relay and the most oxidized active site redox couple (O/I). This step determines the rate of turnover in both directions, so that the catalytic bias of MeHydA is not determined by the ratio k_2/k_{-2}, but rather by the ratio k_{-1}/k_1. Since this ratio equates $\exp(F/RT(E^0_1 - E^0_R))$, it means that, in the particular case of MeHydA, the potential difference between the relay and one of the two active site one-electron potential determines the catalytic bias of the wild type enzyme.

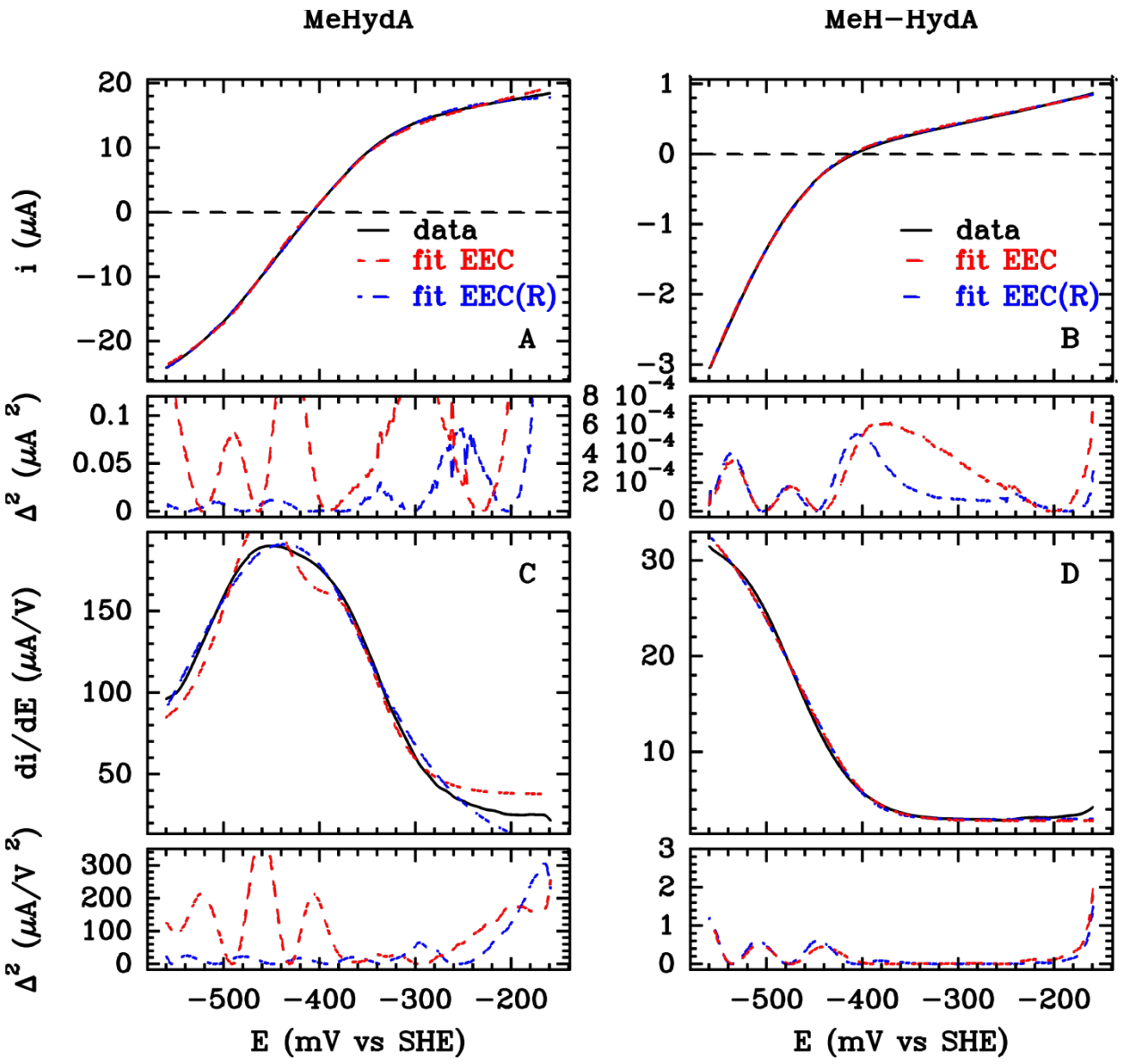

Figure 3: Catalytic signals (H_2 oxidation at high potential, and production at low potential) for MeHydA and MeH-HydA. MeHydA (left) and MeH-HydA (right) are covalently attached to a rotating disc graphite electrode (plain black lines). T = 20°C, pH 7, 1 bar H_2, ω = 3 krpm, 20 mV/s. Panels A and B show the steady-state voltammograms (after correction for the capacitive current) and panels C and D the first derivative of the data. The dashed red and blue lines are the best fits using the EEC and EEC(R) models, respectively, defined in refence.[40,42] The small panels show the residues for each fit. The values of the optimized parameters are listed in Supporting Information, Table S4.

To determine whether the above conclusion holds over a range of experimental conditions, we performed and interpreted a series of experiments that consisted in recording the steady-state voltammetric responses of both MeHydA and MeH-HydA at pH values from 6.5 to 8.5 and H_2 partial pressures in the range 0.18 to 1 bar. For each set of experimental conditions the EEC model was fitted to the voltammetric data of the MeH-HydA enzyme to determine the two active site redox potentials, and these values were used to constrain the fit of the EEC(R) model to the MeHydA voltammograms recorded under the same conditions, to obtain the values of E^0_R and k_2/k_{-2}. The fits are all shown in SI Figures S9 and S10. Figure 4A shows the values of E^0_1, E^0_2 and E^0_R obtained at different H_2 concentrations against pH, and panel B shows the values of k_2/k_{-2}. Dark symbols correspond to data recorded 100% H_2, lighter symbols show the values obtained from the data recorded under 55%, 35% and 18% H_2; a small offset along the X-axis decreases the overlap between the data points recorded at the same pH. We observed the following features. First, the catalytic bias of the WT enzyme in favor of H_2 reduction, defined as the ratio of the limiting currents in the two directions of the reactions (and determined from the

extrapolation of the current calculated with the EEC(R) model) increases when the H_2 concentration is raised and when the pH is decreased. This is as observed before for various NiFe and FeFe hydrogenases[37,45–47] including MeHydA.[48] The following analysis clarifies why this occurs in the case for MeHydA and shows that this is not merely due to substrate availability. Second, the value of k_2/k_{-2} (Fig. 4B) increases in proportion to H+ concentration (one hundred fold over 2 pH units) and decreases when [H_2]; this variation is not unexpected considering that k_{-2} includes H_2 binding, and it suggests that k_2 includes protonation (this is consistent with the observation that E^0_2 is independent of pH, meaning that not all intramolecular electron transfer steps are coupled to protonation, hence one proton must be taken up after the full oxidation of the active site). Below we show that k_2/k_{-2} is not the determinant of the bias. Third, the value of E^0_1 (green in Fig. 4A) decreases exactly 60mV per pH unit (green dotted line) as expected for a one-electron one-proton reaction. This is true at all H_2 concentrations. Fourth, the values of E^0_2 is less pH-dependent (-20mV/pH, blue dotted line) and independent of [H_2]. Fifth, the value of E^0_R shows little dependence on pH under 100% H_2 (-24mV/pH), and a slightly larger pH dependence at lower H_2 concentrations (up to -30mV/pH under 18% H_2, still much less than the -60mV/pH expected for a fully coupled electron/proton transfer; the small pH dependence may be due to the fits of the data recorded under low [H_2] being less reliable). A small dependence of the potential on pH is what we expect for a FeS cluster involved in electron transfer, and we consider that this observation validates the theoretical models and methods used here. We note that the pH 8 value of E^0_R = -440 mV is not far from the value of -370 mV obtained from EPR titrations for the FS4A and FS4B clusters of CpI hydrogenase. [49]

Fig. 5 shows the relation between the catalytic bias, k_2/k_{-2} (circles) and k_{-1}/k_1 (squares), for all data. The dashed red line shows y=x, and matches the values of k_{-1}/k_1, showing that the latter determines the bias. This confirms the above conclusion that the catalytic bias of the WT enzyme is determined by the kinetics of intramolecular electron transfer, and this is so over a large range of experimental conditions.

Discussion

We have thus been able to engineer the [FeFe]-hydrogenase from *M. elsdenii*, MeHydA, to generate a significantly shorter variant, MeH-HydA, which lacks the N-terminal ferredoxin domain. Even though the deletion accounts for only 15% of the protein, it is the first attempt to go in this direction. More extensive deletion might be considered in the future. The protein expresses and folds well and is highly active after maturation. As shown by FTIR, EPR and Mössbauer spectroscopic characterization, the H-cluster correctly assembles in MeH-HydA, with spectroscopic properties almost identical to those of MeHydA and CrHydA. The only remarkable difference distinguishing MeH-HydA from the other [FeFe]-hydrogenases is the deviating EPR spectrum of the Hox-CO state (Figures 2b and S6) which is less anisotropic.

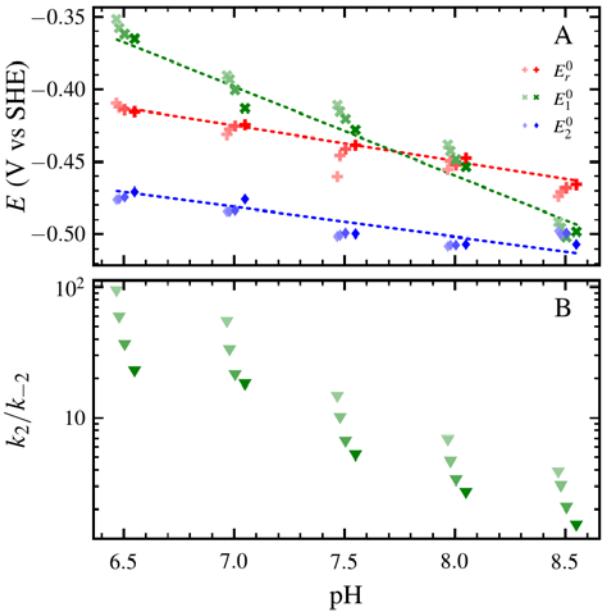

Figure 4: The parameters obtained from fitting the EEC and EEC(R) models to steady-state voltammograms obtained with MeH-HydA and MeHydA in a range of pH (6.5 to 8.5) and H_2 concentration (from 10% to 100%). The potentials of the active site and of the relay (panel A) and the "intrinsic" bias of the active site, k_2/k_{-2}, as defined in Fig. S8 and in ref [44]. See Figs S9 and S10. Dark symbols correspond to values obtained from the data recorded under 100% H_2, and lighter symbols indicate H_2 partial pressures of 0.55, 0.3 and 0.18 bar. T=20°C, ω = 3 krpm, 20 mV/s. Data obtained at different H_2 concentrations are slightly offset along the pH axis for clarity.

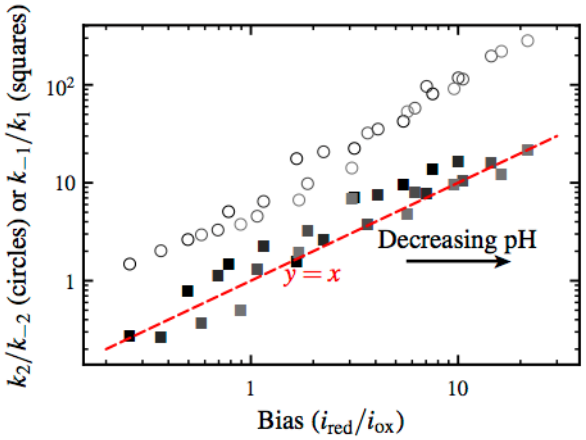

Figure 5: Evidence that the catalytic bias (the ratio of limiting currents) is determined by k_{-1}/k_1 over a large range of pH values and [H_2] concentrations. Fitted values of k_2/k_{-2} (circles) or k_{-1}/k_1 (squares) (k_2 and k_{-1} are both in the direction of H_2 evolution in the scheme of Fig. S8) plotted against the experimental value of the catalytic bias (i_{red}/i_{ox}) for different values of the pH and of the partial pressure of H_2 (from 100% dark symbols to 18%, light grey symbols). Data obtained in the pH range 6.5 (rightmost) to 8.5 (leftmost) from experiments using

MeH-HydA and MeHydA. The y=x line is shown as a dashed red line.

An interesting result of our study is that, when adsorbed onto the surface of an electrode, MeH-HydA displays some resistance to oxygen. This is intimately related to the fact, observed here for the first time, that the hydrogenase precursor (MeHydA), is more resistant to gaseous inhibitors (O_2, CO) than other HydAs (this work and previous reports), and that a high degree of resistance is conserved upon truncation.

First, regarding the kinetics of inhibition by CO, while there was no qualitative difference between MeHydA, CrHydA and CaHydA[36] , we observed significant quantitative differences. Indeed, the rate of CO binding was up to 40-fold and 4-fold lower than that obtained in the case of CrHydA and CaHydA respectively and it was even 500-fold lower than in the case of DdHydAB (Table S3). The rate of CO binding/release depends on the kinetics of both long-range CO diffusion within the enzyme and CO binding at the active site.[17,40] Since the latter is expected to be the same in all HydAs, we consider as likely that the difference in binding/release kinetics reveals significant differences in intramolecular diffusion rates. Which amino-acids are responsible for making intramolecular diffusion so slow in MeHydA is now being investigated further in our groups.

Second, the reaction of MeHydA with O_2 appears to follow the same mechanism as that previously described for CaHydA and CrHydA[13,17] as well as for *Acetobacterium woodii* HydA.[37] The value of the rate constant k_{in}^{O2}, which depends on O_2 intramolecular diffusion through the protein and binding at the distal Fe of the H-cluster[17], is at least 10-fold lower than in any other HydA (Table 1). Considering the above conclusion that the intramolecular diffusion of CO is particularly slow in MeHydA, it is reasonable to assume that this is also the reason why O_2 inhibition is slow. However, the initial O_2 binding step is not the parameter that strictly defines the "overall" sensitivity to O_2, because what matters is the rate of irreversible formation of the inactive forms, which is the effective 2nd-order rate defined by $k_{eff}=k_{in}^{O2}\cdot k_3/(k_a+k_3)$ whose calculated values are shown in Table 1.[42] The k_{eff} value is about the same for MeHydA and CaHydA despite the fact that the individual rate constants are significantly different. In particular, the smaller value of k_{in}^{O2} in MeHydA is compensated for by the smaller value of k_a and the larger value of k_3. According to the model in ref[17] , these two rate constants correspond to the complex redox chemistry of the O_2 bound adduct and have no simple meaning. They can be affected by electron availability as well as the kinetics of proton transfer in the enzyme.

We show here that MeH-HydA and MeHydA display comparable reactivities with respect to the gaseous inhibitors CO and O_2. A recent related report using a truncated form of CaHydA describes similar observations, even though this work suffers from incomplete characterization of the truncated form of CaHydA.[23] This together with the observation that CrHydA, lacking accessory clusters, and DdHydAB, containing two ferredoxin-type clusters, are both very sensitive to CO and O_2, show that previous suggestions regarding the protective role of the accessory clusters from O_2 might not be necessarily correct in the case of [FeFe]-hydrogenases.[17] This obviously indicates that understanding O_2 sensitivity of HydAs remains challenging. Nevertheless, MeH-HydA is much more O_2-resistant than CrHydA (Figure 2 and Table 1), thus showing that it is possible to engineer a complex HydA enzyme to generate a simple, active and significantly O_2-resistant CrHydA-like enzyme, which was one of the objectives of this work.

Figure 3 clearly shows that both MeHydA and MeH-HydA forms are biased in the direction of H_2 production (the catalytic currents are larger in the direction of reductive catalysis), but unexpectedly MeH-HydA much more so than MeHydA. Since the active site is not affected by the truncation, a major role of the iron-sulfur electron transfer chain of MeHydA in tuning the enzyme's catalytic bias is inferred. Comparing the results of the fits for the two versions of the same enzyme (with and without the relays) tells us why the catalytic bias is changed. In MeH-HydA, the catalytic bias is simply $i_{red}/i_{ox} = k_2/k_{-2} \simeq 15$ at pH 7, 100% H_2 (Figures 3 and S8), with k_2 (in the direction of H_2 evolution) and k_{-2} being the rate constants that define the chemical (as opposed to redox) steps in the catalytic cycle. The ratio k_2/k_{-2} is therefore a property of the active site. Our data show that this ratio is about the same for MeH-HydA and for MeHydA, again in agreement with the truncation having no significant effect on the active site. However, in the case of MeHydA, the intramolecular electron transfer step (between the relay and the active site, k_1 and k_{-1} in Figure S8) is slow and fully determines the catalytic rates in both directions. As a consequence, the catalytic bias for MeHydA is instead given by the ratio k_{-1}/k_1, which is determined by the difference between the potential of the relay and that of a particular one-electron redox reaction at the active site. Here, $i_{red}/i_{ox} = k_{-1}/k_1 = \exp(F/RT(E^0_1 - E^0_R)) \simeq 2$ at pH 7, 100% H_2, with E^0_1 being the potential of one of the two redox transitions of the active site and E^0_R the potential of the relay. (Note that the equation above is *not* the same as eq. 4 in ref [50], which tentatively links the bias to the difference between E^0_R and the open circuit potential.) The slow intramolecular ET step compensates for the strong "intrinsic" preference of the active site to catalyse H_2 production over H_2 oxidation, and entirely defines the catalytic bias. We have shown (see the discussion of Figs 4 and 5) that this is true over a large range of pH and [H_2].

In that regard, it is interesting to parallel our observations to a recent analysis of two HydAs, named CpI and CpII, within *C. pasteurianium*.[51] CpI has extremely high hydrogen production activity in comparison to CpII, while CpII has elevated hydrogen oxidation activity in comparison to CpI, thus with biases in tight relation with their respective physiological functions. How the bias is tuned in these enzymes is unclear but it is tempt-

ing to relate it, at least in part, to the established absence of a ferredoxin domain and accessory factors in CpII, like in MeH-HydA, which are present in CpI. This finally further illustrates the notion, previously raised in the case of [NiFe]-hydrogenases[52], that the bias may not be mainly determined by redox properties of the active site but rather by reaction steps occurring on sites that are remote from the active site. However, the mechanism that selects the catalytic bias is unprecedented: in NiFe hydrogenases, the rate limiting step is not the same when the enzyme evolves or oxidizes H_2, and site-directed mutations that block the gas channel[52] or slow intermolecular electron transfer[53] selectively slow the rate of the step that limits H_2 evolution or H_2 oxidation, respectively.[54] Regarding MeHydA the data are consistent with intramolecular electron transfer being rate limiting in both directions of the reactions over a range of experimental conditions, and the rate of this particular step determining the catalytic bias (Fig. 5).

This is certainly a new research direction that can be further addressed using the interesting pair of enzymes MeHydA and MeH-HydA.

Conclusion

All these data show that it is possible to engineer HydAs to generate active hydrogenases that combine the resistance of the most resistant HydAs and the simplicity of algal HydAs, containing only the H-cluster. They also clearly establish that the accessory clusters, at least in MeHydA, are key molecular components for defining the catalytic bias due to the slow and limiting intramolecular electron transfers. In contrast, at least when the enzyme is attached to an electrode surface, they play no role in controlling the sensitivity to O_2. Whether this can be generalized to other HydAs remains to be shown. These engineered enzymes thus provide unique tools to further study basic issues, such as the tunability of their catalytic bias.

ASSOCIATED CONTENT

Supporting Information. Sequence alignment of CpI with MeHydA and MeH-HydA, purification profiles of apo- and FeS-MeH-HydA, EPR, Mössbauer spectra, chronoamperometry of CO inhibition and additional tables.
This material is available free of charge via the Internet at http://pubs.acs.org.

AUTHOR INFORMATION

Corresponding Author

* marc.fontecave@college-de-france.fr

Present Addresses

†Biochemistry of Gas-Converting Biocatalysts, Department of Chemistry, Technische Universitaet Berlin, Max-Volmer-Laboratorium, Strasse des 17. Juni 135, 10623 Berlin, Germany.

Author Contributions

The manuscript was written through contributions of all authors. / All authors have given approval to the final version of the manuscript. / ‡These authors contributed equally.

ACKNOWLEDGEMENTS

The Fondation de l'Orangerie for individual Philanthropy, the French State Program 'Investissements d'Avenir (Grants "LABEX DYNAMO", ANR-11-LABX-0011, and "LABEX ARCANE", ANR-11-LABX-0003-01) supported this work. The authors thank Pr. Philippe Soucaille for his contribution to this work through helpful discussions and JW Peters for providing CrHydA-expressing plasmid.
The project leading to this publication has received funding from Excellence Initiative of Aix-Marseille University - A*MIDEX, a French "Investissements d'Avenir" programme.The French authors are part of the French bioinorganic chemistry research network (www.frenchbic.cnrs.fr).

References

(1) Lubitz, W.; Ogata, H.; Rüdiger, O.; Reijerse, E. *Chem. Rev.* **2014**, *114*, 4081–4148.

(2) Peters, J. W.; Schut, G. J.; Boyd, E. S.; Mulder, D. W.; Shepard, E. M.; Broderick, J. B.; King, P. W.; Adams, M. W. W. *Biochim. Biophys. Acta* **2015**, *1853*, 1350–1369.

(3) Peters, J. W.; Lanzilotta, W. N.; Lemon, B. J.; Seefeldt, L. C. *Science* **1998**, *282*, 1853–1858.

(4) Nicolet, Y.; Piras, C.; Legrand, P.; Hatchikian, C. E.; Fontecilla-Camps, J. C. *Struct. Lond. Engl. 1993* **1999**, *7*, 13–23.

(5) Berggren, G.; Adamska, A.; Lambertz, C.; Simmons, T. R.; Esselborn, J.; Atta, M.; Gambarelli, S.; Mouesca, J.-M.; Reijerse, E.; Lubitz, W.; Happe, T.; Artero, V.; Fontecave, M. *Nature* **2013**, *499*, 66–69.

(6) Esselborn, J.; Lambertz, C.; Adamska-Venkatesh, A.; Simmons, T.; Berggren, G.; Noth, J.; Siebel, J.; Hemschemeier, A.; Artero, V.; Reijerse, E.; Fontecave, M.; Lubitz, W.; Happe, T., *Nat. Chem. Biol.* **2013**, *9*, 607–609.

(7) Adamska-Venkatesh, A.; Roy, S.; Siebel, J. F.; Simmons, T. R.; Fontecave, M.; Artero, V.; Reijerse, E.; Lubitz, W. *J. Am. Chem. Soc.* **2015**, *137*, 12744–12747.

(8) Silakov, A.; Wenk, B.; Reijerse, E.; Lubitz, W. *Phys. Chem. Chem. Phys.* **2009**, *11*, 6592.
(9) Caserta, G.; Adamska-Venkatesh, A.; Pecqueur, L.; Atta, M.; Artero, V.; Souvik, R.; Reijerse, E.; Lubitz, W.; Fontecave, M. *Biochim. Biophys. Acta BBA - Bioenerg.* **2016**, *1857*, 1734-1740
(10) Mulder, D. W.; Boyd, E. S.; Sarma, R.; Lange, R. K.; Endrizzi, J. A.; Broderick, J. B.; Peters, J. W. *Nature* **2010**, *465*, 248–251.
(11) Caserta, G.; Pecqueur, L.; Papini, C.; Fontecave, M. *Encyclopedia of Inorganic and Bioinorganic Chemistry*; Scott, R. A., Ed.; John Wiley & Sons, Ltd: Chichester, UK, 2017; pp 1–18.
(12) Artero, V.; Berggren, G.; Atta, M.; Caserta, G.; Roy, S.; Pecqueur, L.; Fontecave, M. *Acc. Chem. Res.* **2015**, *48*, 2380–2387.
(13) Orain, C.; Saujet, L.; Gauquelin, C.; Soucaille, P.; Meynial-Salles, I.; Baffert, C.; Fourmond, V.; Bottin, H.; Léger, C. *J. Am. Chem. Soc.* **2015**, *137*, 12580–12587.
(14) Swanson, K. D.; Ratzloff, M. W.; Mulder, D. W.; Artz, J. H.; Ghose, S.; Hoffman, A.; White, S.; Zadvornyy, O. A.; Broderick, J. B.; Bothner, B.; King, P.W.; Peters, J.W. *J. Am. Chem. Soc.* **2015**, *137*, 1809–1816.
(15) Lambertz, C.; Leidel, N.; Havelius, K. G. V.; Noth, J.; Chernev, P.; Winkler, M.; Happe, T.; Haumann, M. *J. Biol. Chem.* **2011**, *286*, 40614–40623.
(16) Stripp, S. T.; Goldet, G.; Brandmayr, C.; Sanganas, O.; Vincent, K. A.; Haumann, M.; Armstrong, F. A.; Happe, T. *Proc. Natl. Acad. Sci.* **2009**, *106*, 17331–17336.
(17) Kubas, A.; Orain, C.; De Sancho, D.; Saujet, L.; Sensi, M.; Gauquelin, C.; Meynial-Salles, I.; Soucaille, P.; Bottin, H.; Baffert, C.; Fourmond, V.; Best, R.B. ; Blumberger, J.; Léger, C. *Nat. Chem.* **2016**, 9, 88-95.
(18) Stanley, J. L.; Rauchfuss, T. B.; Wilson, S. R. *Organometallics* **2007**, *26*, 1907–1911.
(19) Mulder, D. W.; Ortillo, D. O.; Gardenghi, D. J.; Naumov, A. V.; Ruebush, S. S.; Szilagyi, R. K.; Huynh, B.; Broderick, J. B.; Peters, J. W. *Biochemistry*, **2009**, *48*, 6240–6248.
(20) Baba, T.; Ara, T.; Hasegawa, M.; Takai, Y.; Okumura, Y.; Baba, M.; Datsenko, K. A.; Tomita, M.; Wanner, B. L.; Mori, H. *Mol. Syst. Biol.* **2006**, *2*, 1-11.
(21) Cherepanov, P. P.; Wackernagel, W. *Gene* **1995**, *158*, 9–14.
(22) Girbal, L.; von Abendroth, G.; Winkler, M.; Benton, P. M. C.; Meynial-Salles, I.; Croux, C.; Peters, J. W.; Happe, T.; Soucaille, P. *Appl. Environ. Microbiol.* **2005**, *71*, 2777–2781.
(23) Gauquelin, C.; Baffert, C.; Richaud, P.; Kamionka, E.; Etienne, E.; Guieysse, D.; Girbal, L.; Fourmond, V.; André, I.; Guigliarelli, B.; Léger, C.; Soucaille, P.; Meynial-Salles, I. *Biochim. Biophys. Acta BBA - Bioenerg.* **2017**, *1859*, 69-77.
(24) Kincade, J. M.; deHaseth, P. L. *Gene* **1991**, *97*, 7–12.
(25) Akhtar, M. K.; Jones, P. R. *Appl. Microbiol. Biotechnol.* **2008**, *78*, 853–862.
(26) Atta, M.; Meyer, J. *Biochim. Biophys. Acta* **2000**, *1476*, 368–371.
(27) Loiseau, L.; Ollagnier-de Choudens, S.; Lascoux, D.; Forest, E.; Fontecave, M.; Barras, F. *J. Biol. Chem.* **2005**, *280*, 26760–26769.
(28) Fish, W. W. *Methods Enzymol.* **1988**, *158*, 357–364.
(29) Beinert, H. *Anal. Biochem.* **1983**, *131*, 373–378.
(30) Reijerse, E.; Lendzian, F.; Isaacson, R.; Lubitz, W. *J. Magn. Reson.* **2012**, *214*, 237–243.
(31) Pilbrow, J. R. *Appl. Magn. Reson.* **1996**, *10*, 45–53.
(32) Fourmond, V.; Lautier, T.; Baffert, C.; Leroux, F.; Liebgott, P.-P.; Dementin, S.; Rousset, M.; Arnoux, P.; Pignol, D.; Meynial-Salles, I.; Soucaille, P.; Bertrand, P.; Léger, C. *Anal. Chem.* **2009**, *81*, 2962–2968.
(33) Fourmond, V. *Anal. Chem.* **2016**, *88*, 5050–5052.
(34) Adamska-Venkatesh, A.; Krawietz, D.; Siebel, J.; Weber, K.; Happe, T.; Reijerse, E.; Lubitz, W. *J. Am. Chem. Soc.* **2014**, *136*, 11339–11346.
(35) Sensi, M.; Baffert, C.; Greco, C.; Caserta, G.; Gauquelin, C.; Saujet, L.; Fontecave, M.; Roy, S.; Artero, V.; Soucaille, P.;

Meynial-Salles, I.; Bottin, H.; de Gioia, L.; Fourmond, V.; Léger, C.; Bertini, L. *J. Am. Chem. Soc.* **2016**, *138*, 13612–13618.
(36) Baffert, C.; Bertini, L.; Lautier, T.; Greco, C.; Sybirna, K.; Ezanno, P.; Etienne, E.; Soucaille, P.; Bertrand, P.; Bottin, H.; Meynial-Salles, I.; de Gioia, L.; Léger, C. *J. Am. Chem. Soc.* **2011**, *133*, 2096–2099.
(37) Ceccaldi, P.; Schuchmann, K.; Müller, V.; Elliott, S. J. *Energy Env. Sci* **2017**, *10*, 503–508.
(38) Rodríguez-Maciá, P.; Reijerse, E.; Lubitz, W.; Birrell, J. A.; Rüdiger, O. *J. Phys. Chem. Lett.* **2017**, *8*, 3834–3839.
(39) Baffert, C.; Demuez, M.; Cournac, L.; Burlat, B.; Guigliarelli, B.; Bertrand, P.; Girbal, L.; Léger, C. *Angew. Chem. Int. Ed.* **2008**, *47*, 2052–2054.
(40) Liebgott, P.-P.; Leroux, F.; Burlat, B.; Dementin, S.; Baffert, C.; Lautier, T.; Fourmond, V.; Ceccaldi, P.; Cavazza, C.; Meynial-Salles, I.; Soucaille, P.; Fontecilla-Camps, J.C.; Guigliarelli, B.; Bertrand, P.; Rousset, M.; Léger, C. *Nat. Chem. Biol.* **2010**, *6*, 63–70.
(41) Frangioni, B.; Arnoux, P.; Sabaty, M.; Pignol, D.; Bertrand, P.; Guigliarelli, B.; Léger, C. *J. Am. Chem. Soc.* **2004**, *126*, 1328–1329.
(42) Fourmond, V.; Léger, C. *Curr. Opin. Electrochem.* **2017**, *1*, 110–120.
(43) Sensi, M.; del Barrio, M.; Baffert, C.; Fourmond, V.; Léger, C. *Curr. Opin. Electrochem.* **2017**, *5*, 135–145.
(44) Fourmond, V.; Baffert, C.; Sybirna, K.; Lautier, T.; Abou Hamdan, A.; Dementin, S.; Soucaille, P.; Meynial-Salles, I.; Bottin, H.; Léger, C. *J. Am. Chem. Soc.* **2013**, *135*, 3926–3938.
(45) Léger, C.; Jones, A. K.; Roseboom, W.; Albracht, S. P. J.; Armstrong, F. A. *Biochemistry*, **2002**, *41*, 15736–15746.
(46) Murphy, B. J.; Sargent, F.; Armstrong, F. A. *Energy Env. Sci* **2014**, *7*, 1426–1433.
(47) Lampret, O.; Adamska-Venkatesh, A.; Konegger, H.; Wittkamp, F.; Apfel, U.-P.; Reijerse, E. J.; Lubitz, W.; Rüdiger, O.; Happe, T.; Winkler, M. *J. Am. Chem. Soc.* **2017**, *139*, 18222–18230.
(48) Butt, J. N.; Filipiak, M.; Hagen, W. R. *Eur. J. Biochem.* **1997**, *245*, 116–122.
(49) Artz, J. H.; Mulder, D. W.; Ratzloff, M. W.; Lubner, C. E.; Zadvornyy, O. A.; LeVan, A. X.; Williams, S. G.; Adams, M. W. W.; Jones, A. K.; King, P. W.; Peters, J.W. *J. Am. Chem. Soc.* **2017**, *139*, 9544–9550.
(50) Hexter, S. V.; Grey, F.; Happe, T.; Climent, V.; Armstrong, F. A. *Proc. Natl. Acad. Sci.* **2012**, *109*, 11516–11521.
(51) Therien, J. B.; Artz, J. H.; Poudel, S.; Hamilton, T. L.; Liu, Z.; Noone, S. M.; Adams, M. W. W.; King, P. W.; Bryant, D. A.; Boyd, E. S.; Peters, J.W. *Front. Microbiol.* **2017**, *8*, 1305.
(52) Abou Hamdan, A.; Dementin, S.; Liebgott, P.-P.; Gutierrez-Sanz, O.; Richaud, P.; De Lacey, A. L.; Rousset, M.; Bertrand, P.; Cournac, L.; Léger, C. *J. Am. Chem. Soc.* **2012**, *134*, 8368–8371.
(53) Dementin, S.; Belle, V.; Bertrand, P.; Guigliarelli, B.; Adryanczyk-Perrier, G.; De Lacey, A. L.; Fernandez, V. M.; Rousset, M.; Léger, C. *J. Am. Chem. Soc.* **2006**, *128*, 5209–5218.
(54) del Barrio, M.; Sensi, M.; Orain, C.; Baffert, C.; Dementin, S.; Fourmond, V.; Léger, C. *Acc. Chem. Res.* **2018**, *51*, 769-777.

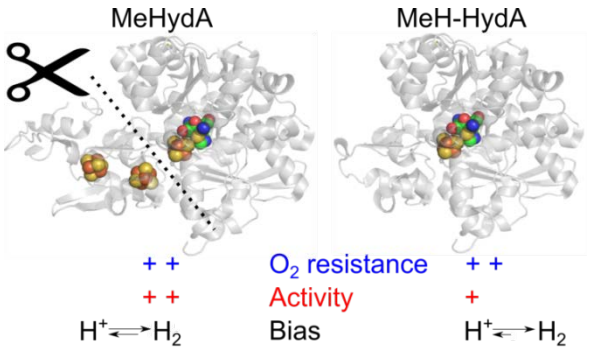
MeHydA
MeH-HydA
+ +
+ +
$H^+ \rightleftharpoons H_2$
O_2 resistance
Activity
Bias
+ +
+
$H^+ \rightleftharpoons H_2$

Supplementary Information

Engineering an [FeFe]-hydrogenase:

do accessory clusters influence O_2 resistance and catalytic bias ?

Giorgio Caserta,[a1] Cecilia Papini,[a1] Agnieszka Adamska-Venkatesh,[b] Ludovic Pecqueur,[a] Constanze Sommer,[b] Edward Reijerse,[b] Wolfgang Lubitz,[b] Charles Gauquelin,[c] Isabelle Meynial-Salles,[c] Debajyoti Pramanik,[d] Vincent Artero,[d] Mohamed Atta,[d] Melisa del Barrio,[c] Bruno Faivre,[a] Vincent Fourmond,[e] Christophe Léger,[e] Marc Fontecave[a*]

[a] Laboratoire de Chimie des Processus Biologiques, Collège de France, Université Pierre et Marie Curie, CNRS UMR 8229, PSL Research University, 11 place Marcelin Berthelot,75005 Paris, France

[b] Max-Planck-Institut für Chemische Energiekonversion, Stiftstrasse 34-36, 45470 Mülheim an der Ruhr, Germany.

[c] LISBP, Université de Toulouse, CNRS, INRA, INSA, Toulouse, France

[d] Laboratoire de Chimie et Biologie des Métaux, Université Grenoble Alpes, CEA/BIG, CNRS, 17 rue des martyrs, 38000 Grenoble, France

[e] Aix Marseille Univ., CNRS, BIP UMR 7281, Marseille, France.

* to whom correspondence should be addressed : marc.fontecave@college-de-france.fr; tel : (33) 144271360

[1] GC and CP contributed equally to this work

Figures

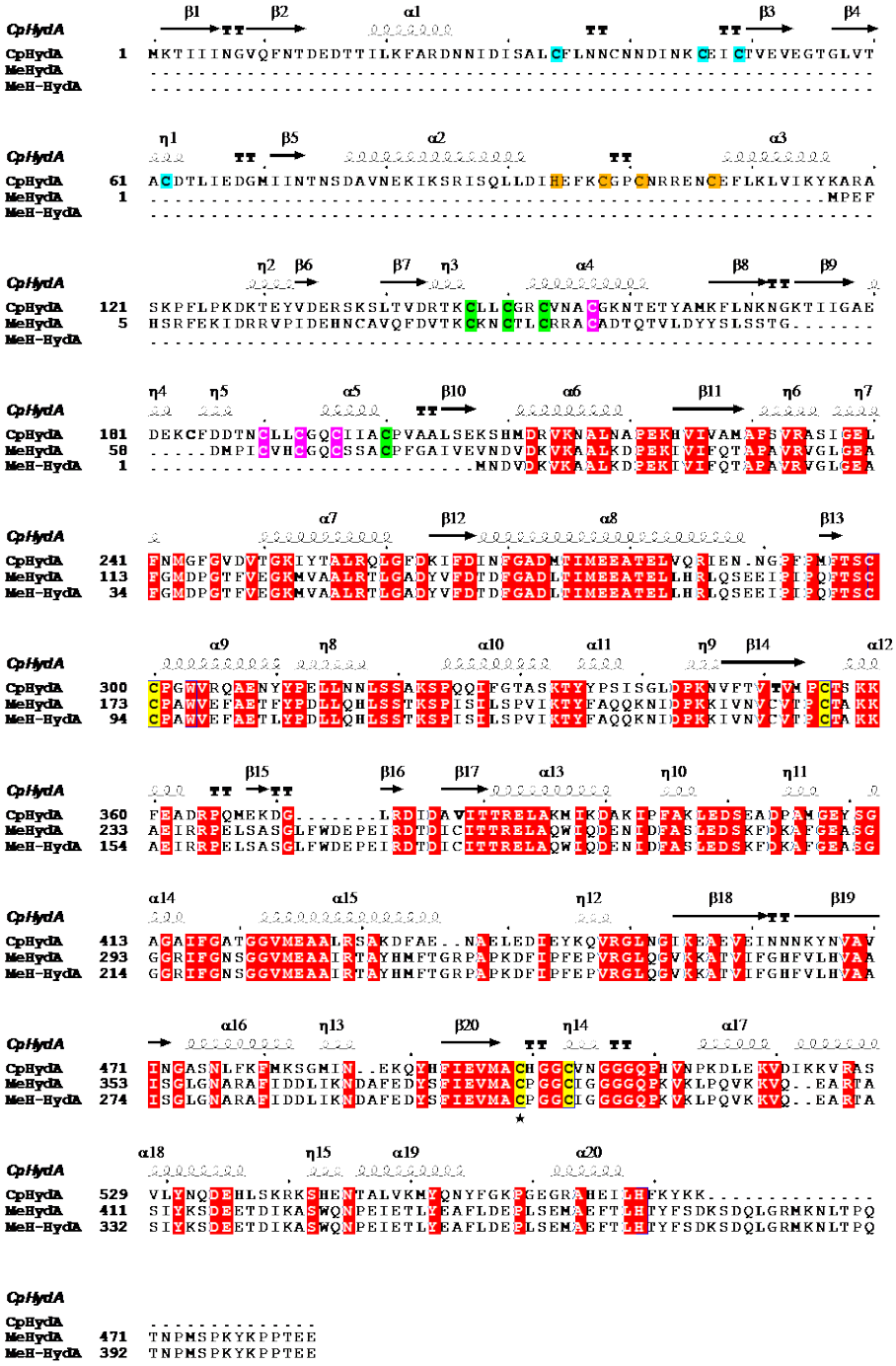

Figure S1 : Sequence alignment of CpHydA, MeHydA and MeH-HydA proteins using clustalO.[1] Secondary structures are calculated using the crystal structure of CpHydA (pdb 3c8y). The cysteine residues chelating the $[4Fe\text{-}4S]_H$ cluster are highlighted in yellow with the cysteine linking the 2Fe-subcluster marked with a star; conserved residues are highlighted in red. Cysteines boxed in cyan coordinate the [2Fe-2S] cluster in CpHydA. Residues boxed in orange, green and magenta coordinate the auxiliary [4Fe-4S] clusters. The figure was generated with ESPript3.[2]

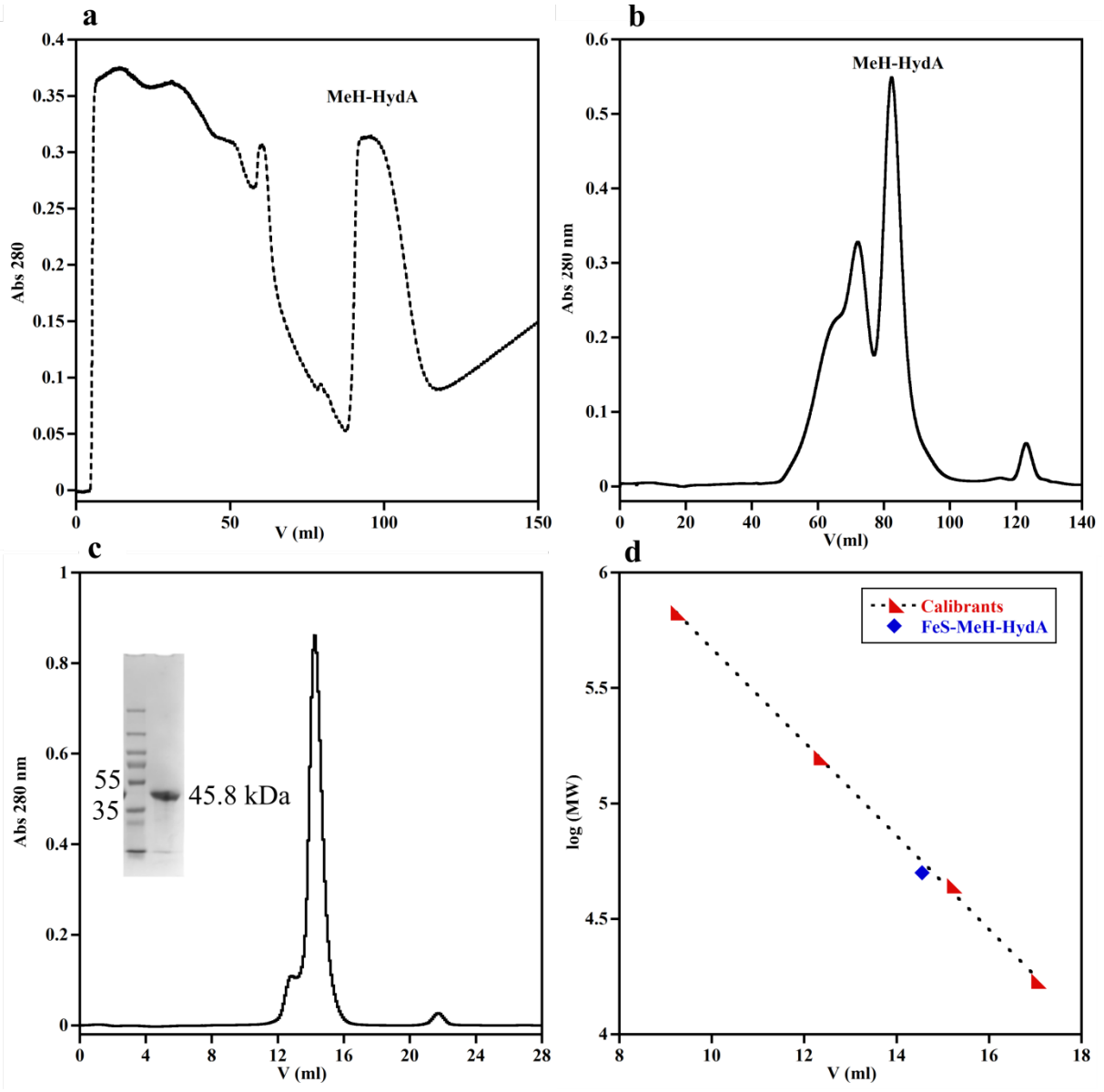

Figure S2: Apo-MeH-HydA purification. Apo-MeH-HydA was purified to homogeneity in two chromatographic steps (**a** and **b**). **a**) Ni-NTA chromatography elution profile using an imidazole gradient. **b**) Size exclusion chromatography elution profile on a Superdex S200 16/600 in 50 mM Tris-HCl buffer pH 8.0, 200 mM NaCl, 5 mM DTT. **c**) Anaerobic size exclusion chromatography elution profile on an analytical Superdex S200 10/300 in 50 mM Tris-HCl pH 8.0 containing 300 mM NaCl, 10% glycerol and 5 mM DTT. The elution volume of the apo-MeH-HydA is 14.55 mL. The inset displays a SDS gel after chromatography. **d**) Superdex S200 10/300 GL calibration curve using Thyroglobulin (670 kDa, 9.22 mL), γ-globulin (158 kDa, 12.32 mL), Ovalbumin (44 kDa, 15.2 mL) and Myoglobin (17 kDa, 17.03 mL). The derived molecular weight suggests that apo-MeH-HydA is monomeric.

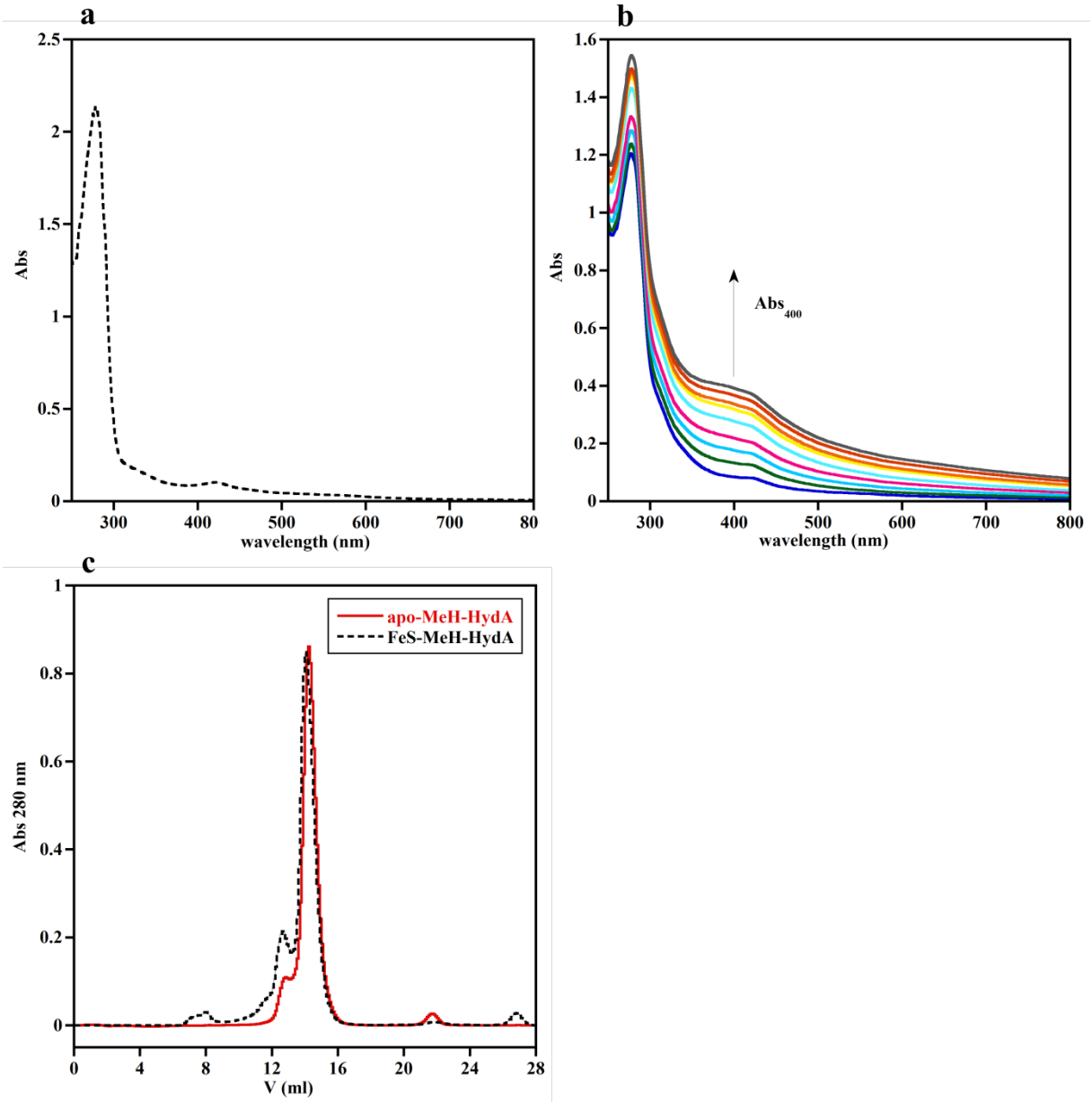

Figure S3: [Fe–S] reconstitution of apo-MeH-HydA. **a**) UV-visible spectrum of 25 µM apo-MeH-HydA in 25 mM Tris-HCl pH 8.0, 200 mM NaCl, 5 mM DTT in a 1 cm pathlength cuvette. **b**) UV-visible absorption spectra of 100 µM MeH-HydA recorded every 20 minutes during [Fe-S] cluster reconstitution. Reaction mixture (100 µM apo MeH-HydA in the presence of 5 molar excess of Fe (II) and L-cysteine, 10 mM DTT and a catalytic amount of cysteine desulfurase) in 50 mM Tris pH 8, 300 mM NaCl, 10% v/v glycerol using a 1 mm pathlength cuvette. **c**) S200 elution profile of apo-MeH-HydA (red) and FeS-MeH-HydA (dashed black).

a)

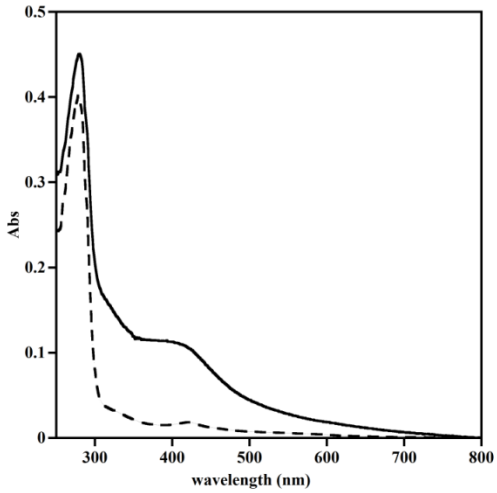

b)

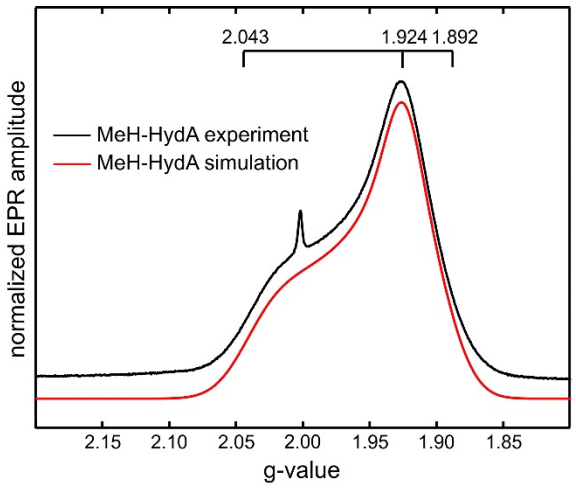

c)

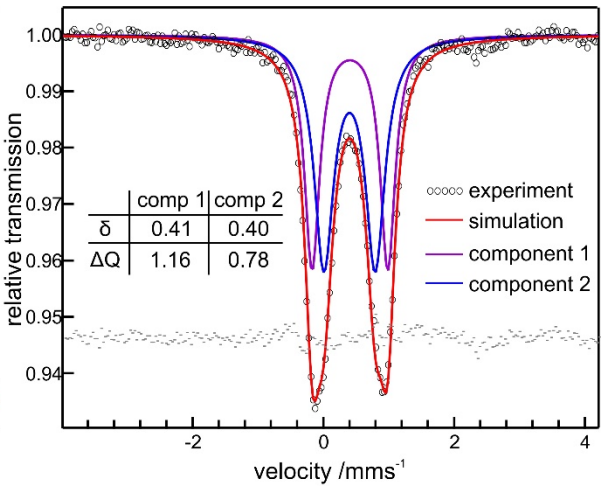

Figure S4: Spectroscopic properties of [FeS]-reconstituted MeH-HydA. a) UV-visible spectra of apo and [FeS]-reconstituted protein b) Q-band FID-detected EPR spectra measured at 10K of reduced (10mM NaDT) protein together with simulation. G-values are given at the top of figure. c) Mössbauer spectrum of [^{57}FeS]-reconstituted MeH-HydA measured at 160K in zero magnetic field. Spectrum was simulated with two components with equal contribution. Parameters given in the figure are in mm/s. The grey horizontal bars represent the residual of the fit shifted into the vertical range of the experimental Mössbauer spectra.

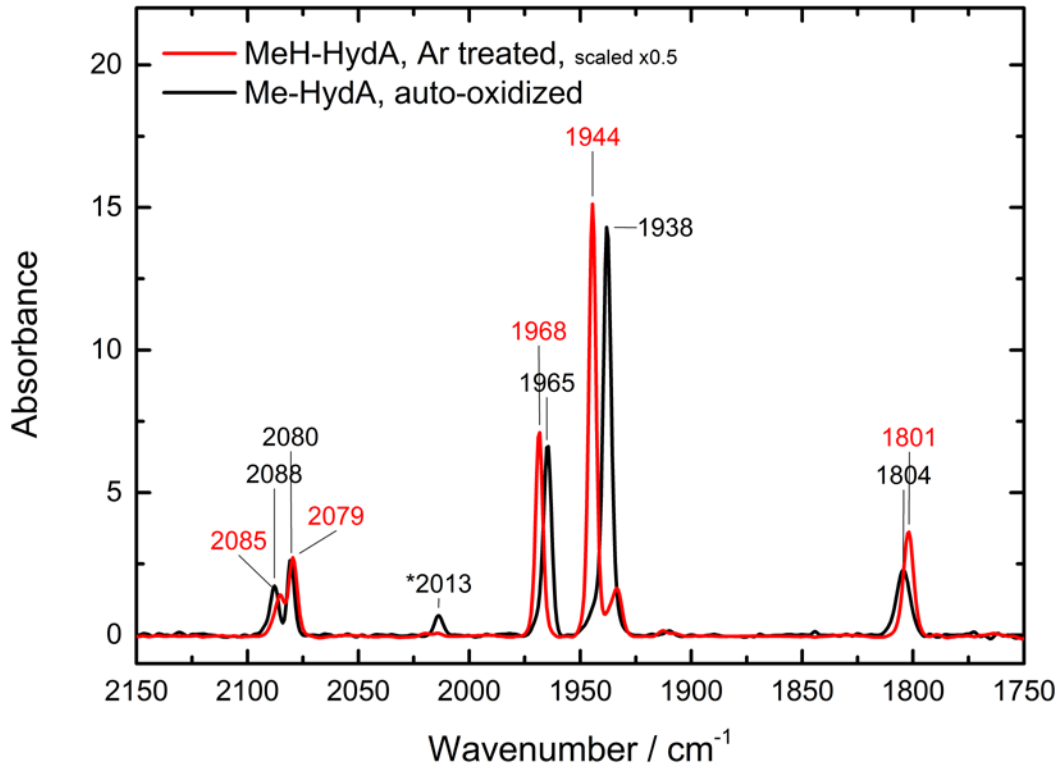

Figure S5: FTIR spectra of MeH-HydA (red) and MeHydA (black) in the Hox state. The feature at 2013 cm^{-1} (*) shows the presence of small amounts of Hox-CO state in MeHydA.

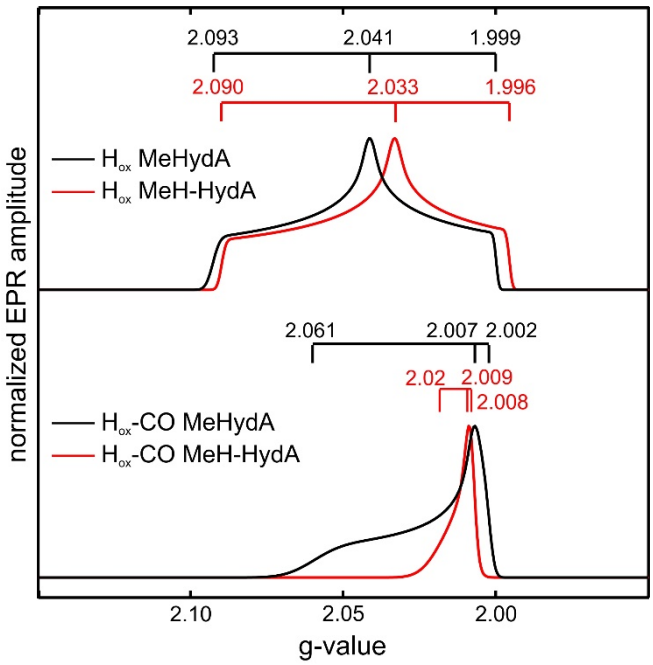

Figure S6: Comparison of simulations of EPR spectra obtained for MeHydA and MeH-HydA in H_{ox} and H_{ox}-CO states. g-values used for simulations are given above the spectra.

For MeH-HydA in the H_{ox} state a slight shift of the g-values (up to 0.008) is observed with respect to MeHydA. This shift can be explained by slightly different geometry of the H-cluster. In the spectrum of the Hox-CO state of MeH-HydA all the lines are collapsing creating a very narrow spectrum which was not observed for any of the other known hydrogenase species. However, the relaxation properties are similar to those of other hydrogenases. This unusual behaviour cannot be explained at the moment considering the fact that the FTIR spectrum obtained for this redox state is identical to those of other [FeFe]-hydrogenases.

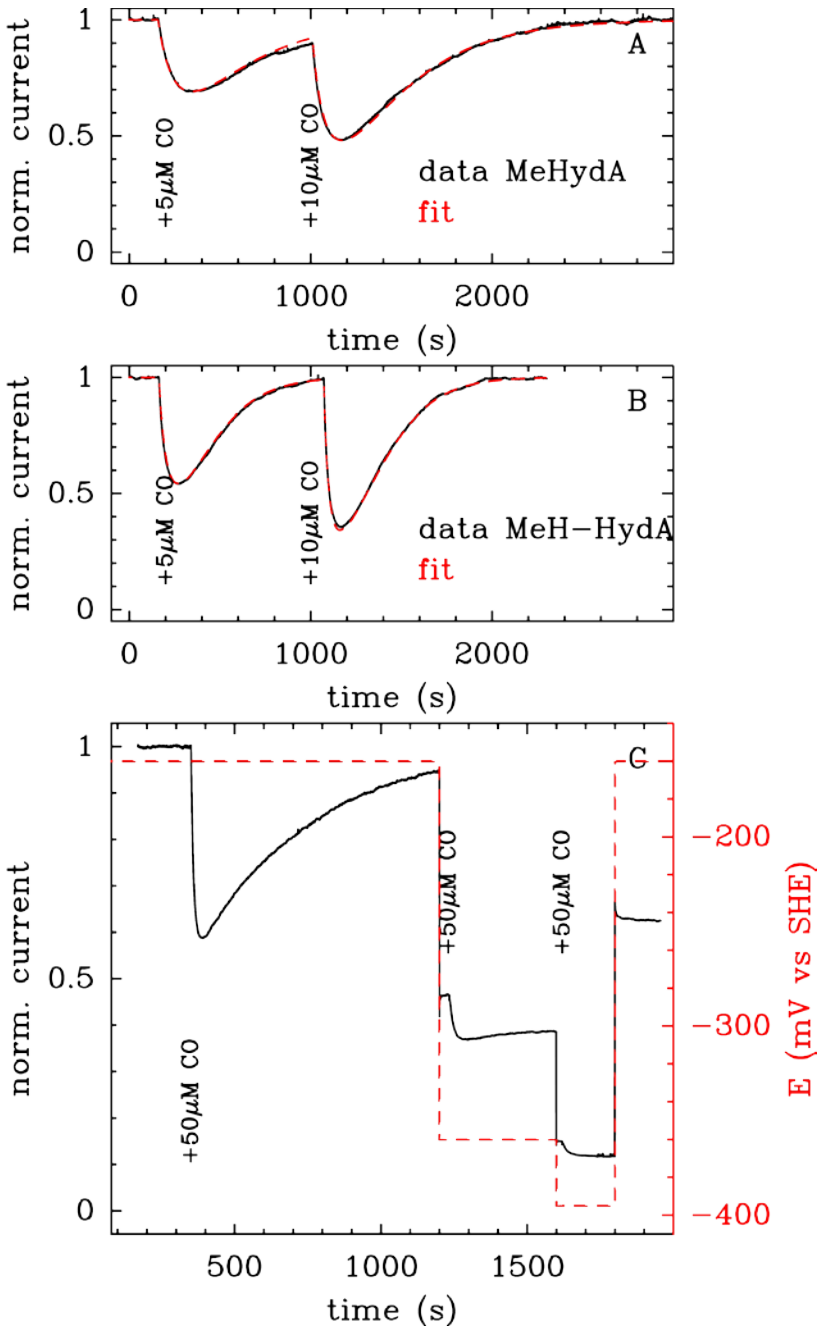

Figure S7: Reversible inhibition by CO. Panel A: reaction of MeHydA with CO at pH 7, E= -160 mV vs SHE, 20°C. The black line is the current normalized by its value before CO is added, corrected for film loss. The red line is the fit to the model in ref [3] , used to measure the kinetic constants for CO binding and release. Panel B: same experiment as in Panel A but carried out with MeH-HydA. Panel C: reaction of MeHydA with CO at pH 7, 1 bar H_2, 20°C, showing that the reaction with CO is less reversible at lower potential (note that all potentials used here are above the open circuit potential; the lower the potential the lower the H_2-oxidation catalytic current). The electrode potential was stepped as indicated by the red dashed line and the right axis.

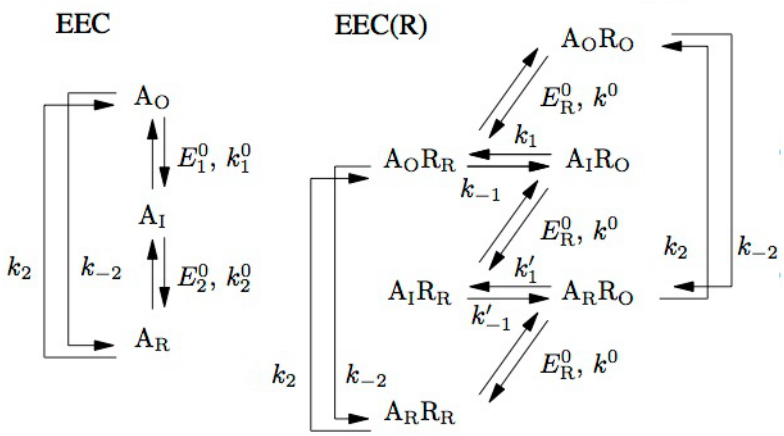

Figure S8: The kinetic schemes used here and described in refs [4,5]

The schemes and the following text are copied from [4] (© 2013 American chemical society, with permission). The letter A with a subscript O (for oxidized"), I (intermediate), or R (reduced) depicts the redox state of the active site. In the rightmost scheme, "R" is the relay that can be either oxidized or reduced. Each redox step ("E") might be coupled to reversible chemical reactions (not depicted), which are supposed to be very fast on the time scale of turnover, and therefore at equilibrium. This may include (de)protonations and/or the binding and release of the substrate/product. Such fast-coupled reactions affect the apparent values of the reduction potentials and the apparent rates of interfacial ET. The catalytic cycles are closed by reversible chemical reactions ("C"), whose first-order (or pseudo-first-order) rates $k_{\pm 2}$ are allowed to be slow on the time scale of turnover. For these reactions, positive subscripts correspond to the catalytic cycle turning in the direction that reduces the substrate (e.g., H_2 evolution in the case of hydrogenases). The pH and substrate/product concentrations are not explicitly considered, but, of course, they may affect the parameters of the model.

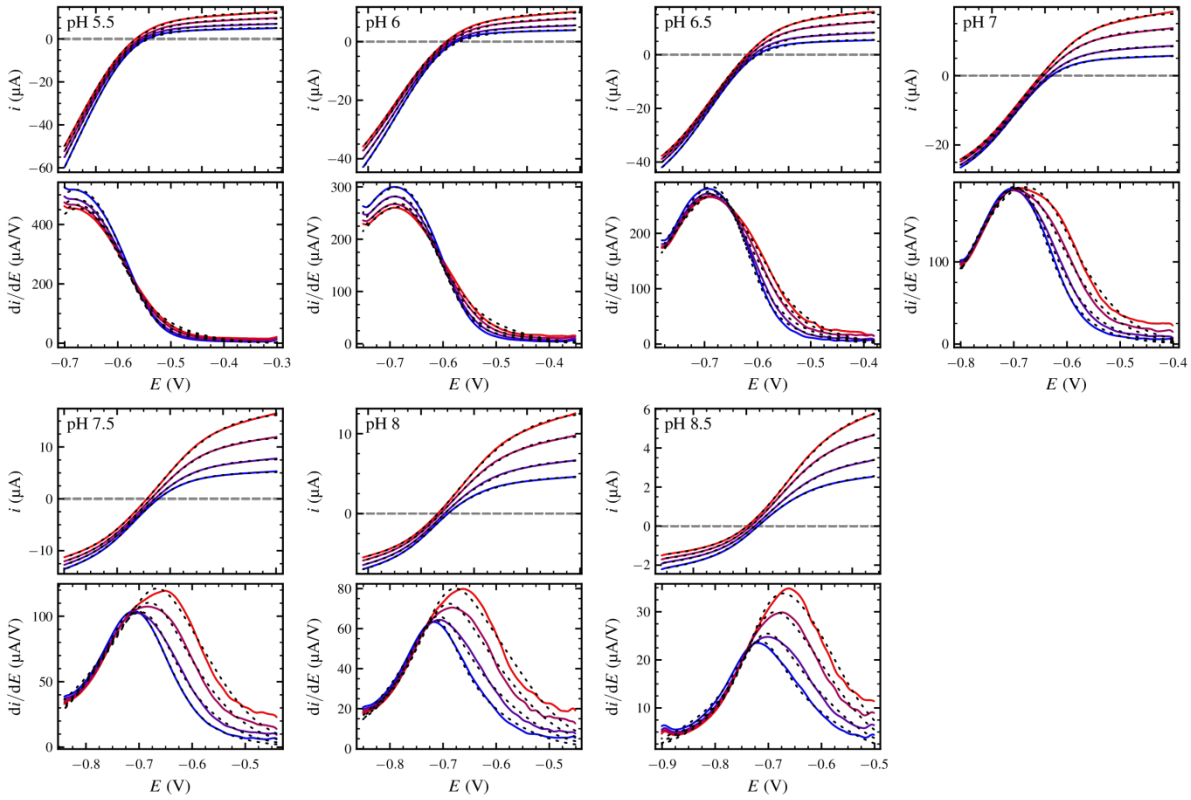

Figure S9: The fits of the EEC(R) model to data recorded with MeHydA in the range of pH 6.5 to 8.5 and H_2 partial pressure 18 (blue) to 100% (red). Data are shown as continuous lines, and the best fits as dotted lines. The best parameters are shown in main text Figures 4 and 5.

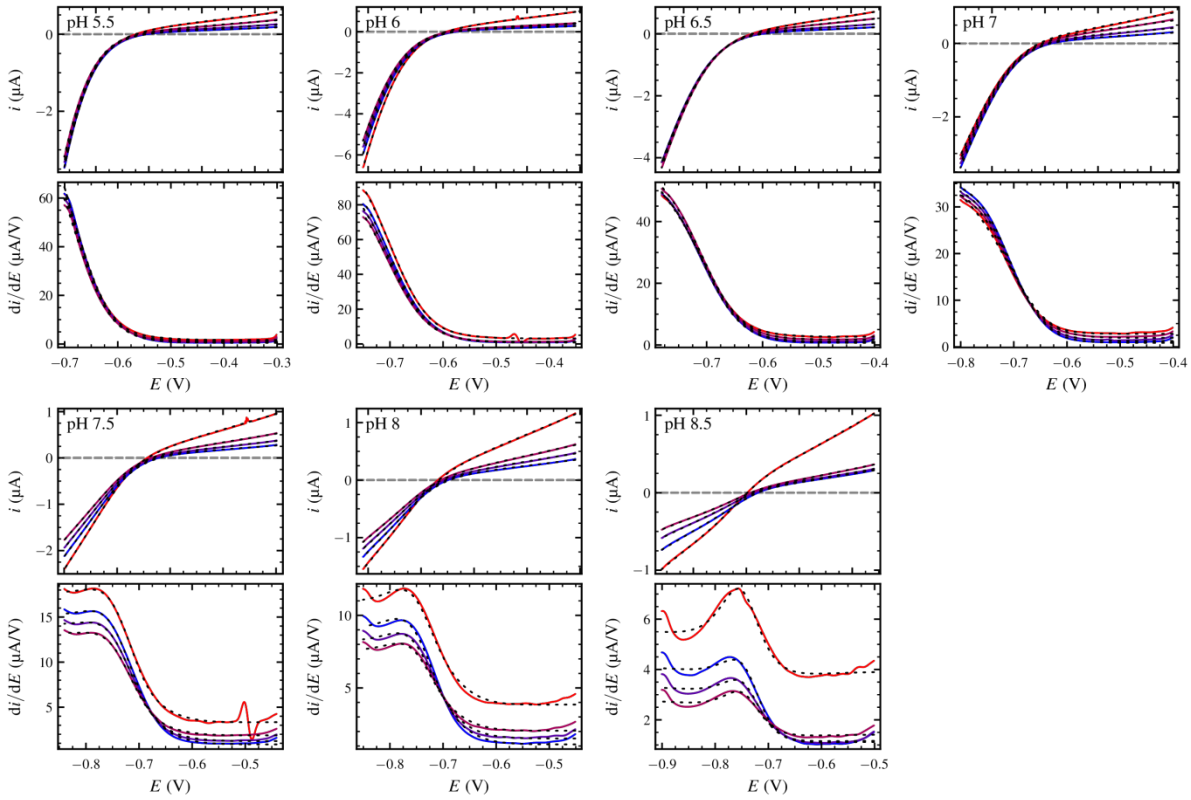

Figure S10: The fits of the EEC model to data recorded with MeH-HydA in the range of pH 6.5 to 8.5 and H_2 partial pressure 18 (blue) to 100% (red). Data are shown as continuous lines, and the best fits as dotted lines. The best parameters are shown in main text Figuress 4 and 5.

Table S1: Specific hydrogenase activity of MeH-HydA depending on different maturation conditions.

pH of maturation	**pH activity**	**T (°C)**	**Specific activity (µmol H_2*mg^{-1}*min^{-1})**	**Incubation time (h)**
8.0**	8.0	21	N.A.	2
6.8	6.8	21	23 ± 3.5	2
8	8	21	N.F	16-24
6.8*	6.8	21	20 ± 2.0*	2
8	6.8	21	2.2 ± 0.3	16-24
6.8	6.8	21	17.5 ± 2.5	16-24
8	8	37	N.A.	16-24
6.8	6.8	37	3.2 ± 0.8	16-24
6.8	6.8	37	2.5 ± 0.5	2
6	6.8	21	125 ± 15	2
6***	6.8	21	80 ± 10	2
6****	**6.8**	**21**	**135 ± 10**	**2**
5.5******	/	/	/	/
5******	/	/	/	/

The data shown are mean values ± s.d. * Maturation has been carried out with 10 molar excess of the hybrid **1**-HydF in the same buffer conditions. ** N.A.=No activity *** The excess of $[Fe_2(adt)(CO)_4(CN)_2]^{2-}$ was increased to 100-fold with respect to protein concentration. In all the other tests the complex was used in a 10-fold excess with respect to protein concentration. **** In bold the best conditions obtained after removing the excess of the chemical. ***** Protein precipitated.

Table S2. FTIR frequencies (in cm^{-1}) corresponding to the CN^- and CO stretching vibrations of CrHydA, MeHydA and MeH-HydA maturated with $[Fe_2(adt)(CO)_4(CN)_2]^{2-}$. In bold, the most characteristic and prominent signals for each redox state.

	state	ν(M-CN⁻)	ν(M-CO)	ν(M-CO-M)	Ref
MeHydA	H_{ox}-CO	2090	**2013**, 1969, 1955	1804	6
	H_{ox}	2087, 2079	1964, **1937**	1803	6
	H_{red}	2069, 2041	1956, 1916, **1891**	-	6
MeH-HydA	H_{ox}-CO	2095, 2089	**2012**, 1970, 1965	1804	this work
	H_{ox}	2089, 2079	1967, **1943**	1801	this work
	$H_{red}/H_{red}H^+$*	-	1985, 1955, 1937, 1896, 1891	-	this work
CrHydA1	H_{ox}-CO	2092, 2084	**2013**, 1970, 1964	1810	7
	$H_{'red'}$-CO	2086, 2075	**2002**, 1967, 1951	1793	7
	H_{ox}	2088, 2072	1963, **1939**	1803	8
	H_{red}	2083, 2067	1962, **1933**	1791	8
	$H_{red}H^+$	2071, 2032	1968, 1914, **1891**	-	8
	$H_{sred}H^+$	2067, 2027	1953, 1917, **1881**	-	8
	H_{hyd}	2082, 2068	1978, **1960**	1860	9

* While some features allow to distinguish the two reduced states (1937 cm^{-1} for H_{red} and 1896 cm^{-1} for $H_{red}H^+$), no clear assignment of the other features can be done at this time.

As far as MeH-HydA is concerned, in the IR traces of Figure 1 one can distinguish the two reduced states (1937 cm^{-1} for H_{red} and 1896 cm^{-1} for $H_{red}H^+$). It is not clear if the doubly reduced state ($H_{sred}H^+$) is present. However, the two overlapping signals at 1896 and 1891 cm^{-1} could correspond to the main signals of both $H_{red}H^+$ and $H_{sred}H^+$. Therefore, there is no possibility for a clear assignment at this point.

Table S3. Kinetic parameters for the inhibition of various HydAs by CO at pH 7.

Enzyme	k_{in}^{CO} [a] $mM^{-1}s^{-1}$	k_{out}^{CO} s^{-1}	T	Ref
MeHydA	2 [a]	0.003	20°C	This work
MeH-HydA	4 [a]	0.005	20°C	This work
CaHydA	8 [a]	0.03	30°C	[10,11]
CrHydA	80 [a]	0.015	30°C	[10]
A. woodii HydA	200 [a]	0.02	30°C	[12]
DdHydAB	1000 [b]	0.03	30°C	[10]

(a) Raw values under 1 atm de H_2, not corrected for the small protective effect of H_2 (b) corrected for the protection by H_2. Note that since the K_m is large and similar for all these enzymes, the correction is small. $k_{in}^{app} = k_{in}^{CO}(\text{no } H_2) / (1+[H_2]/K_m)$.

Table S4. The best parameters of the fits shown in Figure 3, pH 7 100% H_2, as defined in ref [5] and Figure S8.

MeH-HydA in Figs 4B&D, EEC model		MeHydA in Figs 4A&C, EEC(R) model	
E^0_1 (mV vs SHE)	-413	E^0_1 (mV vs SHE) (*)	-411
E^0_2 (mV vs SHE)	-476	E^0_2 (mV vs SHE) (*)	-478 (ill determined)
		E^0_R (mV vs SHE)	-424
k_2/k_{-2}	14	k_2/k_{-2}	17
		k_1/k_2	10^{-6} (very small and ill determined)
		k'_1/k_2	1 (ill determined)
k^0_1/k^0_2	430		
$k_{-2}/(k^0_1\ k^0_2)^{1/2}$	0.005	k_2/k^0_R	1
i_{lim}^{ox}/beta·d_0 (A)	1.5E-7	i_{lim}^{red} (A)	-1.5±0.3 E-5
		beta·d_0	2

(*) in the EEC(R) model, E^0_1 and E^0_2 are related to the parameters defined in fig S8 by:

$E^0_1 = E^0_R - RT/F \log(k_1/k_{-1})$, and $E^0_2 = E^0_R - RT/F \log(k'_1/k'_{-1})$.

The fits can be parameterized using either E^0_1 and E^0_2 or k_1/k_{-1} and k'_1/k'_{-1}.

References:

(1) Sievers, F.; Wilm, A.; Dineen, D.; Gibson, T. J.; Karplus, K.; Li, W.; Lopez, R.; McWilliam, H.; Remmert, M.; Soding, J.; Thompson, J. D.; Higgins, D. G. *Mol. Syst. Biol.* **2014**, *7*, 539.
(2) Robert, X.; Gouet, P. *Nucleic Acids Res.* **2014**, *42* , W320.
(3) Leroux, F.; Dementin, S.; Burlat, B.; Cournac, L.; Volbeda, A.; Champ, S.; Martin, L.; Guigliarelli, B.; Bertrand, P.; Fontecilla-Camps, J.; Rousset, M.; Leger, C. *Proc. Natl. Acad. Sci.* **2008**, *105*, 11188.
(4) Fourmond, V.; Léger, C. *Curr. Opin. Electrochem.* **2017**, *1*, 110.
(5) Fourmond, V.; Baffert, C.; Sybirna, K.; Lautier, T.; Abou Hamdan, A.; Dementin, S.; Soucaille, P.; Meynial-Salles, I.; Bottin, H.; Léger, C. *J. Am. Chem. Soc.* **2013**, *135*, 3926.
(6) Caserta, G.; Adamska-Venkatesh, A.; Pecqueur, L.; Atta, M.; Artero, V.; Souvik, R.; Reijerse, E.; Lubitz, W.; Fontecave, M. *Biochim. Biophys. Acta BBA - Bioenerg.* **2016**, 1857, 1734-1740.
(7) Adamska-Venkatesh, A.; Krawietz, D.; Siebel, J.; Weber, K.; Happe, T.; Reijerse, E.; Lubitz, W. *J. Am. Chem. Soc.* **2014**, *136*, 11339.
(8) Sommer, C.; Adamska-Venkatesh, A.; Pawlak, K.; Birrell, J. A.; Rüdiger, O.; Reijerse, E. J.; Lubitz, W. *J. Am. Chem. Soc.* **2017**, *139*, 1440.
(9) Winkler, M.; Senger, M.; Duan, J.; Esselborn, J.; Wittkamp, F.; Hofmann, E.; Apfel, U.-P.; Stripp, S. T.; Happe, T. *Nat. Commun.* **2017**, *8*, 16115.
(10) Baffert, C.; Bertini, L.; Lautier, T.; Greco, C.; Sybirna, K.; Ezanno, P.; Etienne, E.; Soucaille, P.; Bertrand, P.; Bottin, H.; Meynial-Salles, I.; De Gioia, L.; Léger, C. *J. Am. Chem. Soc.* **2011**, *133*, 2096.
(11) Liebgott, P.-P.; Leroux, F.; Burlat, B.; Dementin, S.; Baffert, C.; Lautier, T.; Fourmond, V.; Ceccaldi, P.; Cavazza, C.; Meynial-Salles, I.; Soucaille, P.; Fontecilla-Camps, J. C.; Guigliarelli, B.; Bertrand, P.; Rousset, M.; Léger, C. *Nat. Chem. Biol.* **2010**, *6*, 63.
(12) Ceccaldi, P.; Schuchmann, K.; Müller, V.; Elliott, S. J. *Energy Env. Sci* **2017**, *10*, 503.